Key Points:
- First ever report of slow-slip event in the Hellenic Subduction System (HSS) prior to a large-magnitude earthquake
- Synergy of upper-plate faulting, slow slip and earthquake swarms tectonically destabilize a subduction-termination prior to the mainshock
- Plate-motion at the western HSS is accommodated by alternating phases of seismic and aseismic slip operating at various depths

Earthquake Swarms, Slow Slip and Fault Interactions at the Western-End of the Hellenic Subduction System Precede the M_w 6.9 Zakynthos Earthquake, Greece

Vasiliki Mouslopoulou[1] , **Gian Maria Bocchini[2]** , **Simone Cesca[3]** ,
Vasso Saltogianni[3] , **Jonathan Bedford[3]** , **Gesa Petersen[3]** , **Michael Gianniou[4,5]** , and
Onno Oncken[3]

[1]National Observatory of Athens, Institute of Geodynamics, Athens, Greece, [2]Institute of Geology, Mineralogy and Geophysics, Ruhr University of Bochum, Bochum, Germany, [3]GFZ Helmholtz Centre Potsdam, German Research Centre for Geosciences, Potsdam, Germany, [4]Hellenic Cadastre, Athens, Greece, [5]University of West Attica, Athens, Greece

Abstract The month-to-year-long deformation of the Earth's crust where active subduction zones terminate is poorly explored. Here we report on a multidisciplinary data set that captures the synergy of slow-slip events, earthquake swarms and fault interactions during the ∼5 years leading up to the 2018 M_w 6.9 Zakynthos Earthquake at the western termination of the Hellenic Subduction System (HSS). It appears that this long-lasting preparatory phase initiated due to a slow-slip event that lasted ∼4 months and released strain equivalent to a ∼M_w 6.3 earthquake. We propose that the slow-slip event, which is the first to be reported in the HSS, tectonically destabilized the upper 20–40 km of the crust, producing alternating phases of seismic and aseismic deformation, including intense microseismicity ($M_w < 4$) on neighboring faults, earthquake swarms in the epicentral area of the M_w 6.9 earthquake ∼1.5 years before the main event, another episode of slow slip immediately preceding the mainshock and, eventually, the large (M_w 6.9) Zakynthos Earthquake. Tectonic instability in the area is evidenced by a prolonged (∼4 years) period of overall suppressed *b*-values (<1) and strong earthquake interactions on discrete strike-slip, thrust and normal faults. We propose that composite faulting patterns accompanied by alternating (seismic/aseismic) deformation styles may characterize multifault subduction-termination zones and may operate over a range of timescales (from individual earthquakes to millions of years).

1. Introduction

Well-monitored examples of large-magnitude earthquakes that rupture subduction plate-boundaries reveal that these earthquakes may be preceded by episodes of slow slip, swarm activity, and/or large foreshocks (i.e., Bouchon et al., 2013; Kato et al., 2012; Schurr et al., 2014). Examples that document such interactions, most of which have been operating on the plate-interface, include the 2011 M_w 9 Tohoku-Oki Earthquake in Japan, the 2012 M_w 7.6 Nicoya Peninsula Earthquake in Costa Rica, and the 2014 M_w 8.1 Iquique megathrust earthquake in Chile (Davis et al., 2015; Kato et al., 2012; Ruiz et al., 2014; Schurr et al., 2014; Uchida et al., 2016). The interrelation, and possible interdependence, of these deformational processes is nevertheless poorly understood, especially in circumstances where upper-plate faulting accommodates a significant percentage of the plate-motion, with the plate-interface playing a secondary role (i.e., Cesca et al., 2017; Mouslopoulou et al., 2019; Wallace et al., 2012). Such settings are often encountered at the terminations of subduction zones (Mouslopoulou et al., 2019), where plate-motion transitions from thrust to strike-slip faulting, producing complex kinematic patterns in the overriding plate (Mann & Frohlich, 1999). The characteristics (duration, size, distribution) of the interplay between the various types of deformation (seismic vs. aseismic) along subduction terminations, especially prior or immediately after large-magnitude earthquakes, is poorly explored mainly due to the lack of relevant data.

The M_w 7.8 Kaikoura Earthquake, that ruptured the southern-end of the Hikurangi margin in 2016 (Cesca et al., 2017), to-date provides the only well-monitored example of a large-magnitude earthquake that ruptured a subduction termination (Mouslopoulou et al., 2019). This earthquake enhanced our understanding of seismogenesis along subduction terminations, as it demonstrated that earthquake-rupture involved

primarily (~80%) slip on upper-plate faults, with only weak triggered seismic-slip and aseismic afterslip on the plate-interface (Mouslopoulou et al., 2019).

On October 25, 2018, a M_w 6.9 earthquake ruptured the western termination of the Hellenic Subduction System (HSS) across a zone where plate-motion transitions from mainly thrust to mainly strike-slip faulting (Royden & Papanikolaou, 2011), providing a valuable new case study of a well-monitored earthquake that ruptures a subduction termination (Figure 1). This earthquake, that occurred southwest of the island of Zakynthos (Chousianitis & Konca, 2019; Sokos et al., 2020) (Figure 1), was preceded by a 5-year-long tectonic instability in the broader epicentral area of the M_w 6.9 event and an intense aftershock sequence (Figures 2 and 3). Here, we report on a multidisciplinary data set of seismological, geodetic, seismic reflection, and bathymetric information that, collectively, capture the earthquake and fault kinematics within this earthquake sequence (hereafter refer to as the Zakynthos Earthquake Sequence [ZES]), prior to and after the main event. We find that alternating phases of aseismic and seismic deformation on the subduction-thrust and the overriding plate, respectively, preceded the M_w 6.9 event and accounted for at least 15% of the relative Eurasian/African plate-motion. The aftershock sequence was accommodated by thrust, strike-slip, and normal faulting in the upper-plate (<20 km) and produced seismic moment equivalent to a M_w 6.2 earthquake (Table S1).

2. The Kinematics of the Western HSS and the M_w 6.9 Zakynthos Earthquake

In the eastern Mediterranean, the oceanic African Plate is being obliquely subducted along the Hellenic margin beneath the continental Eurasian Plate at rates ranging from ~26 to 34 mm/yr (McClusky et al., 2000) (Figure 1). At its western-end, the subduction system terminates against the dextral Kefalonia Transform Fault (Louvari et al., 1999; Sachpazi et al., 2000), transferring its relative plate-motion onto the Apulian collision front (Pérouse et al., 2017) (Figure 1). The kinematic transition from nearly orthogonal convergence (in the south) to pure strike-slip (in the north) is accommodated, along a ~100 km wide zone offshore from western Peloponnese, by strike-slip, thrust and normal faulting (Figure 1). The faults presented in Figure 1 are derived from a combination of published information (Kokkalas et al., 2013; Kokinou et al., 2005; Makris & Papoulia, 2014; Wardell et al., 2014), analysis of bathymetric data (https://portal.emodnet-bathymetry.eu/?menu=19) and reinterpretation of four (Z207, KY301-Z151A/B, KY311, and KY209; for location see Figure 1) published Multi-Channel seismic reflection profiles (Kokkalas et al., 2013; Wardell et al., 2014) (Figure 4).

Beneath western Peloponnese the top of the plate-interface lies at depths between 20 and 40 km and has an average dip of ~17° (Halpaap et al., 2018, 2019; Pearce et al., 2012) (Figures 1 and 3). Just southwest of Zakynthos and proximal to the region of the 2018 mainshock, the plate-interface lies at ~15 km depth (Clément et al., 2000), with a series of east-dipping thrust faults displacing the upper section (<15 km) of the crust and the sea-bed (Kokinou et al., 2005; Louvari et al., 1999; Sachpazi et al., 2000; Wardell et al., 2014). Low-dipping reverse faulting in the area is also supported by moment tensors (MTs) of instrumental seismicity (i.e., Anderson & Jackson, 1987). On the hanging wall of these thrust faults, numerous normal faults have been identified to displace post-Miocene deposits down to depths of at least 10 km (Kokalas et al., 2013; Wardell et al., 2014; this study) (Figure 4).

The 2018 Zakynthos mainshock ruptured the upper <20 km of the crust as a result of shallow thrust and moderately dipping dextral strike-slip faulting (Haddad et al., 2020; Sokos et al., 2020). The focal mechanism presents a large nondouble-couple (non-DC) component with a large negative compensated linear vector dipole indicating a complex rupture process (Sokos et al., 2020). The Global Centroid MT (Global CMT) project suggests a centroid depth for this event of ~16 km and a total seismic-moment release of 2.32×10^{19} Nm (Dziewonski et al., 1981; Ekström et al., 2012). Three past earthquakes with sizes and focal mechanisms similar to that recorded in 2018 have ruptured the crust proximal to Zakynthos over the last ~60 years (in 1959, 1976, and 1997; http://bbnet.gein.noa.gr/HL/). The orientation of their focal mechanisms (Kiratzi & Louvari, 2003; Sokos et al., 2020) is in agreement with the plate-convergence (Figure 1), indicating that these earthquakes accommodated a fraction of the relative African-Eurasian plate-motion. No events greater than M7 have been recorded in the ZES region instrumentally or historically (Papazachos & Papazachou, 2003).
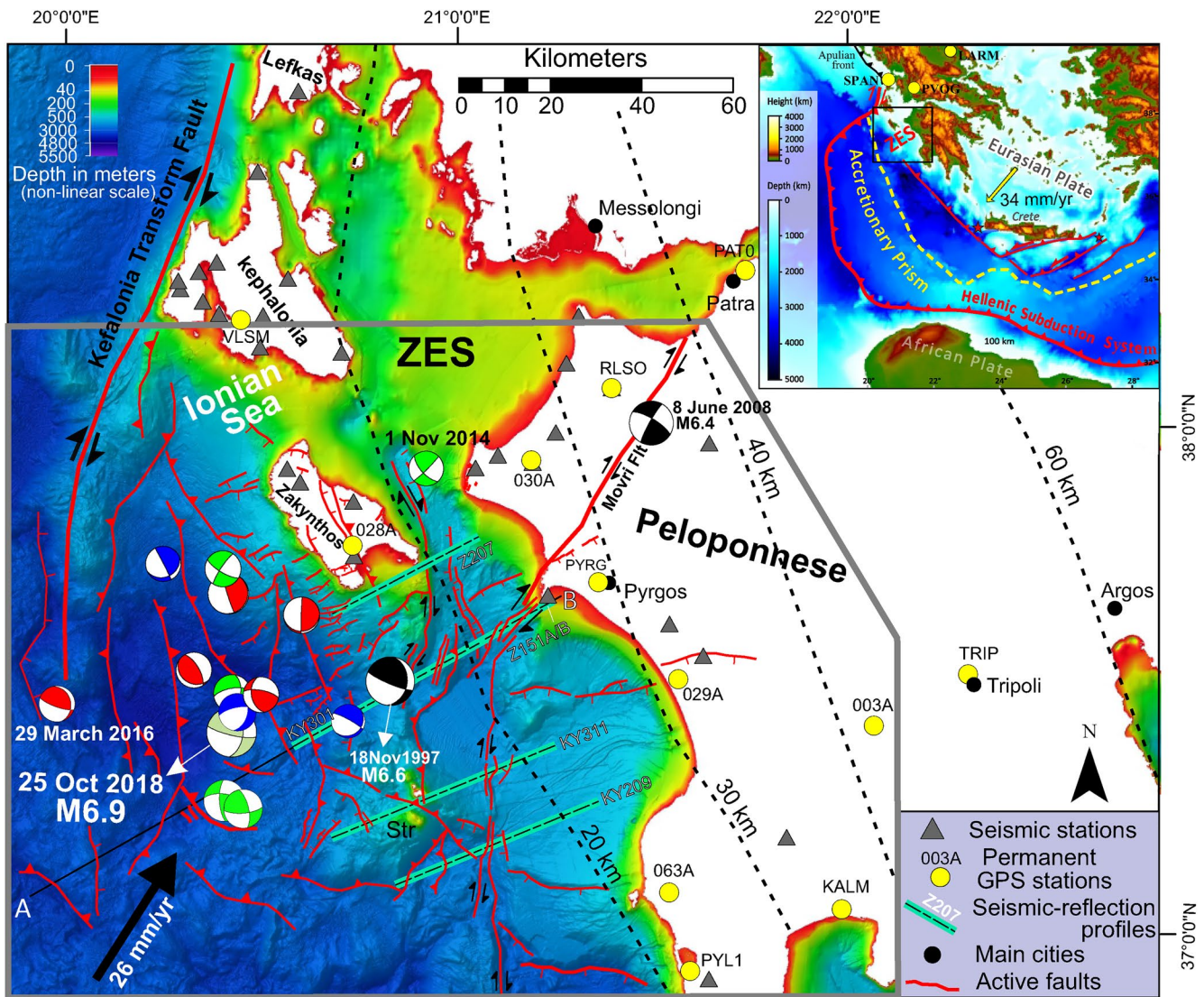
Figure 1. Overview of the kinematics of the study area and the datasets used. Map illustrating the major active faults (indicated by red lines) in the offshore study area and the focal mechanisms of all 14 $M_w \geq 5$ earthquakes that occurred during the ZES, including the M_w 6.9 main event on October 25, 2018, color coded according to fault style (green = strike-slip, blue = normal, red = thrust). Two of these events (indicated) occurred prior to the mainshock. The black moment tensor (MT) solutions indicate the epicenters (ISC-GEM; Storchak et al., 2013) and mechanisms (Global GMT; Dziewonski et al., 1981; Ekström et al., 2012) of the two $M_w > 6$ earthquakes that occurred in the study area during the instrumental period: the 2008 M_w 6.4 Movri Earthquake onshore Peloponnese and the 1997 M_w 6.6 Strofades Earthquake. Gray triangles indicate the seismic stations used for earthquake-relocation and calculation of MT solutions, while yellow-circles localities of permanent GPS stations. Lines Z207, KY301-Z151AB, KY311, and KY209 indicate the localities of the seismic reflection profiles from Wardell et al. (2014) (reinterpreted in Figure 4). The bathymetric profile A-B is presented in Figure S23. Main cities are indicated by black circles. Contours mark the top of the plate-interface (Halpaap et al., 2019). Offshore bathymetry derived from EMODnet (https://portal.emodnet-bathymetry.eu/?menu = 19). Black arrow indicates the relative Eurasia-Africa plate motion (Pérouse et al., 2017). Inset: the study area is located at the western termination of the Hellenic subduction margin, the main tectonic features of which are indicated by red lines. The northward extent of the accretionary prism is indicated by yellow-dashed line. Bathymetry is from GEBCO. Stars indicate the epicenters of the 365AD (west) and 1303AD (east) earthquakes in offshore Crete (map modified from Mouslopoulou et al., 2015). Yellow arrow indicates the relative Eurasia-Africa plate motion as derived from GPS measurements (Saltogianni et al., 2020). Str, Strofades islets. PVOG, SPAN, and LARM are far-field GPS stations (see Section 4.1 for details).

3. The 2014–2019 Zakynthos Earthquake Sequence (ZES)

3.1. Sequence Characteristics

The earthquake sequence analyzed here (lon: 19.5°E to 21.6°E/lat: 36.8°N to 38°N) derives from the Hellenic Unified Seismological Network (HUSN; http://bbnet.gein.noa.gr/HL/) and includes data from the
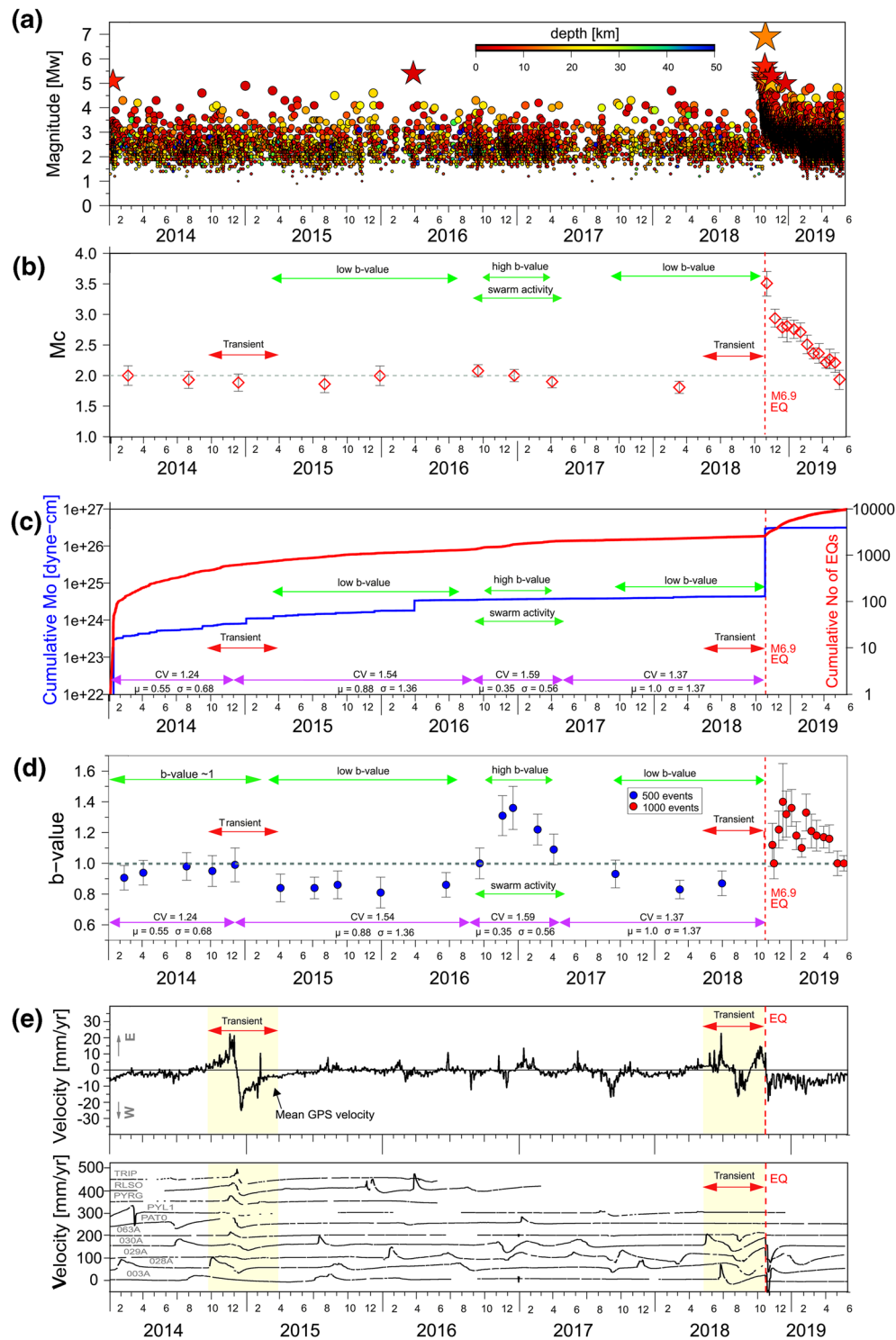
Figure 2. Main characteristics of the seismic and GPS deformation recorded during the ZES. (a) Moment magnitude (M_w) evolution during the ZES. Stars indicate events $M \geq 5$. (b) Evolution of magnitude of completeness (M_c) through time. (c) Cumulative seismic-moment (M_o) and cumulative number of earthquakes during the ZES as a function of time (January 1, 2014 until May 31, 2019). (d) b-value evolution (and its standard deviation) through time. High and low b-values, slow-slip events, and earthquake swarms are indicated on all graphs for comparison. The coefficient of variation (CV) for each time interval is annotated. The average interevent time (days) and the standard deviation are indicated with μ and σ, respectively. (e) Evolution of the East GPS component during the ZES, averaged over the entire GPS network. Lower panel shows individual velocities for selective near-field stations. Trenchward motion is west. The duration of each of the two reported transients is indicated by red arrows (b–d) or yellow shading (e).
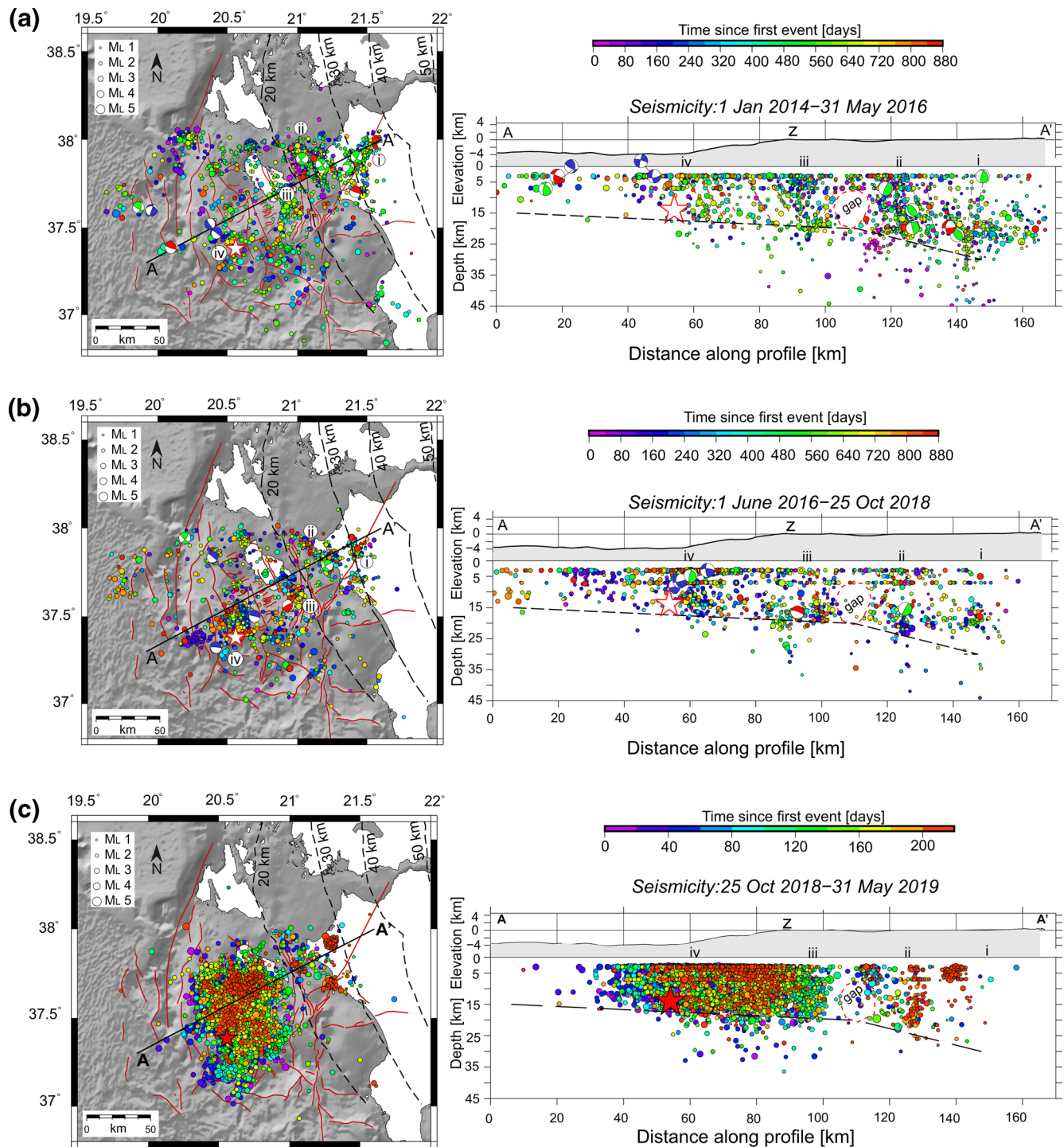
Figure 3. Spatial and temporal distribution of the ZES. Map-view and cross-section of the relocated ZES over three distinct time-intervals: (a) January 1, 2014 to May 31, 2016; (b) June 1, 2016 to October 25, 2018; (c) October 25, 2018 to May 31, 2019. Earthquake activity in each panel is projected along the profile A-A' (70 km either side of the profile) and color-coded according to time (see legend). Seismic events have horizontal and vertical locations errors ≤5 km and root mean square ≤0.5 s. Black dashed-lines in map-view and cross-section indicate the depth-to-the-top of the plate-interface (from Halpaap et al., 2019) while red star indicates the M_w 6.9 epicenter. The 17 focal mechanisms obtained within the pre-October 25, 2018 sequence are color-coded according to fault type (red = thrust, blue = normal, green = strike-slip). Locations i–iv indicate prominent earthquake clusters (see text for discussion). Z, Zakynthos Island. Bathymetry derives from https://www.gmrt.org/.
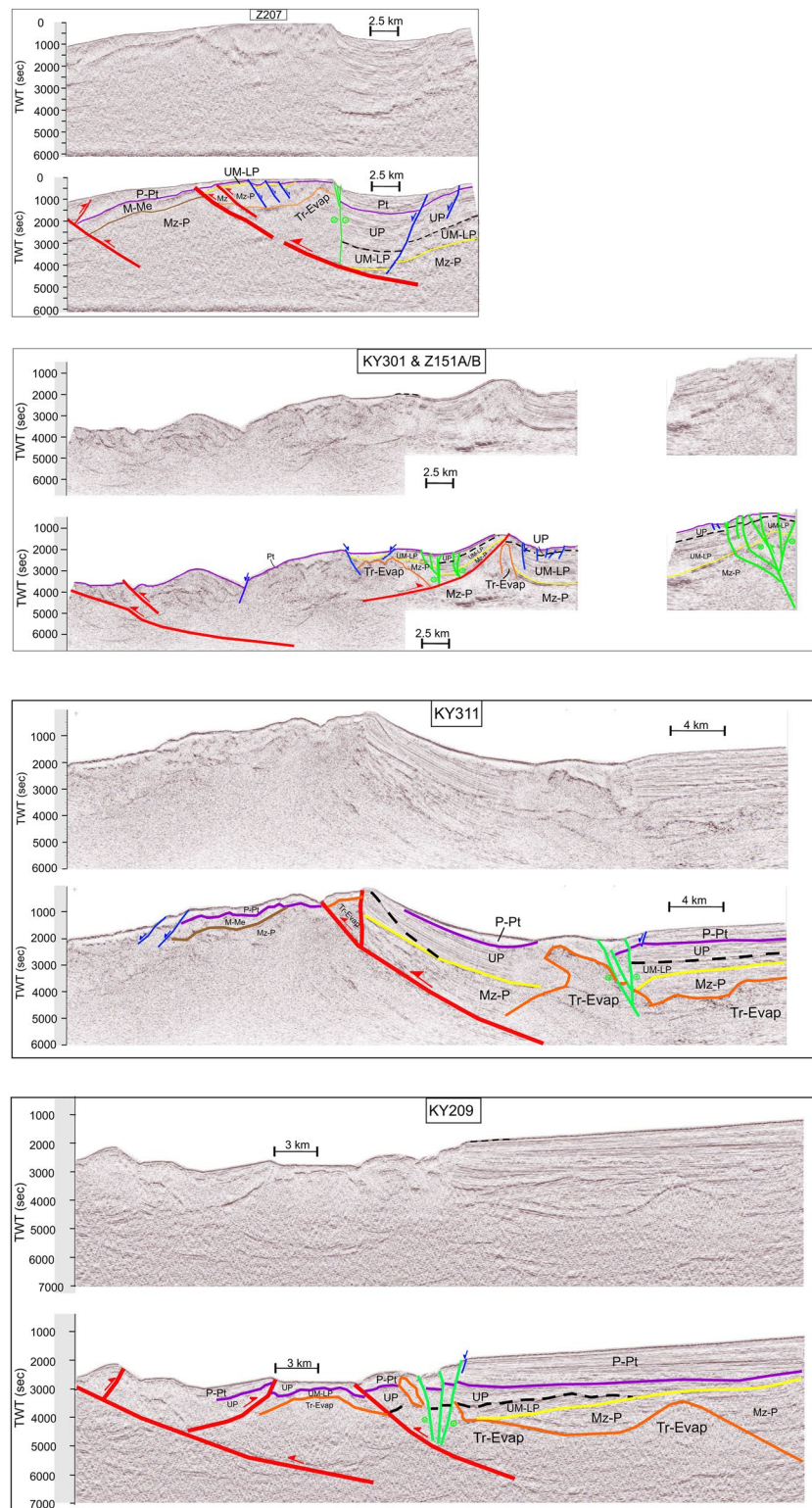
Figure 4. Long-term faulting and kinematics within the ZES. Migrated (top) and reinterpreted (bottom) sections of Multi-Channel seismic reflection profiles Z207, KY301-Z151A/B, KY311, and KY209 from Wardell et al. (2014). Normal (blue), thrust (red), and strike-slip (green) faults are color-coded as per focal mechanisms presented in Figures 3 and 5. M-Me, Miocene and Messinian; Mz-P, Mesozoic-Paleocene; P-Pt, Pliocene-Pleistocene; Tr-Evap, Triassic evaporates (orange); UM-LP, Upper Miocene-Lower Pliocene; UP, Upper Pliocene. The seismic stratigraphy is adopted from Kokkalas et al. (2013).

stations of the National Observatory of Athens (NOA, HL), the University of Patras (HP), the Aristotle University of Thessaloniki (HT), and five additional seismic stations deployed by NOA (HL) in western Peloponnese at different time-periods following the mainshock. The ZES extends over an area of ~18,000 km^2, from northwest Peloponnese to the west of the islands of Zakynthos and Kefalonia (Figures 1 and 3), and spans a time-period of ~5 ½ years (January 01, 2014 to May 31, 2019) (Figure 2a). The ZES includes >12,000 earthquakes (Table S3), with the largest event (M_w 6.9) having occurred ~40 km southwest of the island of Zakynthos on October 25, 2018 (22:54 UTC) due to oblique-thrust faulting (Figure 1; Table S4). About one-third of the events in the ZES occurred prior to the mainshock while two-thirds were aftershocks (Figures 2 and 3). The majority of these earthquakes have magnitudes below 3.5 (Figure 2a). The magnitude of completeness (M_c) in the ZES prior to the mainshock is 2.0 ± 0.1, it abruptly increases to 3.5 after the mainshock (Figure 2b) while it returns to premainshock values (~2.0) about 120 days after the mainshock (Figure 2b).

The seismic-moment (M_0) release during the ZES has not been uniform (Figure 2c). In addition to the energy released during the mainshock, two M_w > 5 earthquakes that occurred on January 11, 2014 (M_w 5.1) and on March 29, 2016 (M_w 5.4) dominate the graph in Figure 2c. A further M_w 4.9 earthquake struck about 30 min before the mainshock (22:22 UTC); however, its seismic-moment is poorly resolved in Figure 2c as it is overprinted by the mainshock's moment release. The total M_0 released in the ~5 years prior to the mainshock is equivalent to a ~M_w 5.8 earthquake, while the cumulative M_0 released during the entire ZES is equivalent to a ~M_w 7 earthquake (Table S1).

Seismicity rates within the ZES also vary through time (Figure 2c). For example, a 6-month interval of increased seismicity (September 2016 to April 2017) is preceded (December 2015 to August 2016) and followed (May 2017 to October 2018) by yearlong periods where the seismicity rates are lower, especially proximal to the epicentral area of the M_w 6.9 earthquake (Figures 2a and 2c and Figure S2). This swarm-like activity initiated ~1.5 years before the mainshock and is characterized by three times higher seismicity rates compared to the preceding and following time-periods, absence of a dominant earthquake at the start of the sequence, spatiotemporally clustered events in the proximity of the (future) mainshock location, and the largest (1.59) coefficient of variation during the ZES (Figures 2c and 2d). These characteristics collectively indicate temporally clustered earthquake activity.

To assess whether these fluctuations in the seismicity rates reflect stress changes within the Earth's crust, we have calculated the evolution of the *b*-value of the Gutenberg-Richter frequency-magnitude distribution in the study area, from January 2013 to May 2019 (Figure 2d and Figure S1c). The *b*-value in a given area describes the relative abundance of small to large-magnitude earthquakes at that location and, thus, any temporal variation in *b*-values is often interpreted to reflect changes in the confining stress within the seismogenic crust (Schorlemmer et al., 2005). Namely, *b*-values have been found to relate inversely to differential stresses, with low (<1) *b*-values often indicating elevated stress while high (>1) *b*-values indicate low/heterogeneous stresses. Here, *b*-values were derived for subsets of 500 earthquakes with half-overlapping time-windows for the foreshock sequence (January 01, 2013 to October 25, 2018) and for subsets of 1,000 events in the aftershock sequence (for more details on the *b*-value calculation refer to Text S1 in the Supporting Information). We find that during the ~70 months preceding the mainshock, *b*-values in the ZES fluctuate over four main time-intervals (Figure 2d and Figure S1c): (i) from January 2013 to December 2014, the *b*-value is uniform and about 1 (0.94 ± 0.09); (ii) from January 2015 to August 2016, the *b*-value drops significantly (as low as 0.81); (iii) from September 2016 to April 2017, there is a sharp increase in the *b*-values (up to 1.36) while (iv) from May 2017 till the mainshock (October 25, 2018), the *b*-value drops again below 1 (average of 0.88 ± 0.08). The mean *b*-value of the aftershock sequence is 1.18 ± 0.12, in agreement with elevated values from other aftershock sequences worldwide (Gulia et al., 2018). In summary, *b*-values in the ZES remained uniform and equal to ~1 during 2013 and 2014 (Figure S1c), while from early 2015 until the mainshock in late 2018, the *b*-values were overall <1, except for the 6-month time-period of the swarm-like activity (Figure 2d). This drop of *b*-values characterizes the ZES seismicity only and does not reflect regional changes in the seismicity of the forearc (Figure S1d). For a sequence such as the ZES, where multiple faults appear to be active simultaneously in the subsurface (Figures 1–4), earthquake relocation is vital, not only because it allows delineation of individual earthquake clusters with discrete faults (Waldhauser & Ellsworth, 2002) but also because it helps identify day-to-month long earthquake interactions between neighboring faults (Mouslopoulou & Hristopulos, 2011).

3.2. Earthquake Relocation

We successfully relocated 12,620 earthquakes that occurred within the ZES from January 01, 2014 until May 31, 2019 (Figure 3), using a local minimum 1-D velocity model (Sachpazi et al., 2000) and manually picked P & S phase onsets determined at the National Observatory of Athens (NOA). The main challenges associated with the relocation arose from the large azimuthal gaps (average > 180°) between the seismic source and the seismographs, the poor station density and the complex velocity structure of the study area (Karastathis et al., 2015). We used a constant Vp/Vs ratio of 1.80 in accordance with other seismological studies in the area (Haddad et al., 2020; Kassaras et al., 2016). Pick quality classes and associated errors derive from NOA (Table S2). Our preferred earthquake location software is the Non Linear Location (NLLoc) (Lomax et al., 2000) that uses a nonlinear location algorithm which is thought to provide more reliable solutions and hypocenter error estimates in case of ill-conditioned locations (such as those encountered within the ZES). For more details on the earthquake relocation refer to Text S2 in the Supporting Information. Overall, the relocation of the ZES reduced the average root mean square from 0.39 (revised NOA catalog) to 0.2, with average horizontal and vertical errors of ∼3.8 km (in Hypo71 format from NLLoc).

The most intriguing finding from the relocation is that, in the foreshock sequence, the vast majority of the earthquakes ruptured the upper 20 km of the crust through four main clusters (i–iv in Figures 3a and 3b), each of which appears to have involved slip on multiple inferred slip surfaces (see red dashed lines in Figure 3a). Our results are broadly consistent with those of Sokos et al. (2020) and Haddad et al. (2020), although these studies focus on subsets of the ZES. Earthquake relocation highlights a prominent gap in the seismicity between Zakynthos and western Peloponnese during the foreshock sequence, at depths ranging from ∼7 to 20 km (Figures 3a and 3b). This feature persists also, perhaps slightly less pronounced, during the aftershock sequence (Figure 3c). To better evaluate possible interrelations between these clusters and assess their impact in the ZES evolution, below we constrain the kinematics of these earthquakes.

3.3. Earthquake Focal Mechanisms

We have obtained the moment tensors (MTs) of 102 earthquakes that occurred during the ZES by inverting regional broadband data and fitting full waveform and amplitude spectra in the time and frequency domain (Cesca et al., 2010, 2013; Heimann et al., 2018; Figures S3–S4, see the Texts S3–S4 in the Supporting Information for more details). The studied earthquakes range in moment magnitude from M_w 3.9 to M_w 6.9, show shallow crustal depths down to about 25 km, and are associated with all types of faulting, with a predominance of strike-slip and thrust mechanisms (Figure 5 and Table S4). Seventeen of these events (Figures 3 and 5) have occurred in the time-period that precedes the main earthquake (October 25, 2018), one is the mainshock and the remaining 84 occurred during the aftershock sequence (Figure 5).

The most interesting result of the MT inversion is that it demonstrates a high variability of MT configurations and faulting style over a quite compact region, extending laterally less than 60 km (Figures 1 and 5). Most of the 102 MT solutions could be classified (Cesca, 2020; see Figure S5) into eight families, each sharing similar focal mechanisms, spanning from pure strike-slip to pure thrust, and normal faulting. The variability in these mechanisms is consistent with a NE-SW trending pressure axes, in agreement with the convergence direction, and a NW-SE tension axis (Figure 5c). This faulting style complexity is supported by offshore seismic reflection profiles (e.g., Kokkalas et al., 2013; Wardell et al., 2014; this study) that indicate abundance of deep-thrust and shallow normal faulting as well as steeply dipping strike-slip faults (Figure 4). This is also evidenced in the diverse present-day crustal stress field inferred from regional-scale inversion of focal mechanisms (Konstantinou et al., 2017). Furthermore, our data support a clear difference among the distribution and predominance of different focal mechanisms before and after the mainshock (Figures 3 and 5). Results suggest the activation of a complex, shallow (<20 km) fault network, and the presence of strong stress heterogeneities, probably induced or enhanced by the occurrence of the M_w 6.9 event in the ZES, which was able to trigger microseismicity across a range of fault geometries and faulting styles (Figure 5c). The average depth of reverse faulting, which occur mostly at the western edge of the hypocentral cloud of the main event, is ∼10 km and probably slightly shallower, since the water column deepens to the west and this may have led to depth overestimation of 2–3 km, while for strike-slip and normal
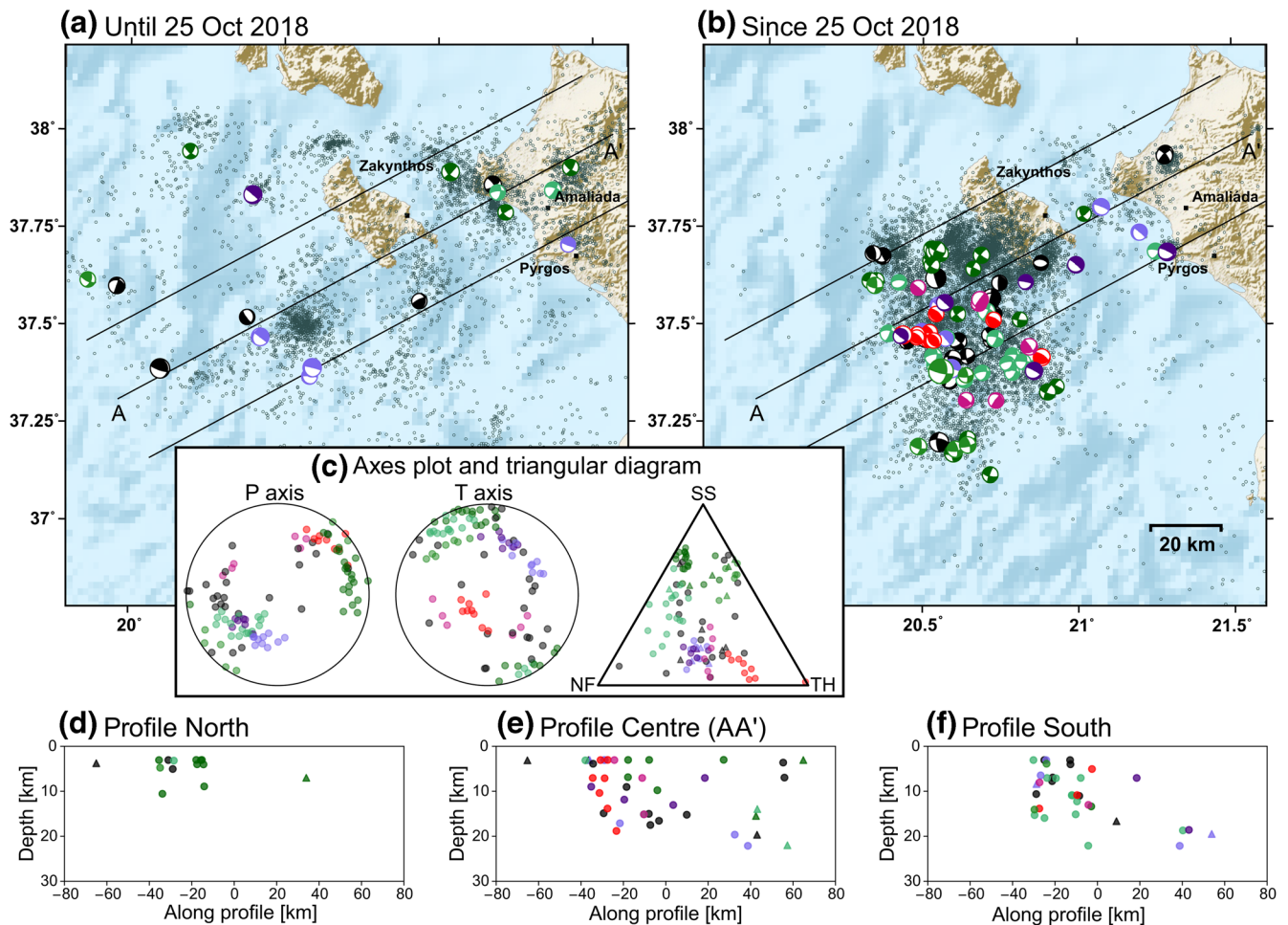
Figure 5. Focal mechanisms within the ZES. Map-view (a and b) and cross-sections (d–f) of 102 focal mechanisms from the ZES. Beachballs are color coded according to eight clusters of earthquakes with similar focal mechanisms, with the colors recalling the fault type (red = thrust, blue = normal, green = strike-slip, and associated shadings when events span various types of faulting; black is used for solutions with unclustered focal mechanisms; see Figure S5 in the Supporting Information for details). The triangle diagram in (c) denotes the kinematics of events analyzed by means of pressure (P) and tension (T) axes orientations and a triangular diagram after Frohlich (1992). Circles in (c–f) indicate events that occurred during the aftershock sequence while triangles represent events that occurred prior to the main event (October 25, 2018). The relocated ZES seismicity is indicated in (a and b) with small gray circles.

faulting, which occurs also east of Zakynthos and on Peloponnese, is ~8 and 9 km, respectively (Table S4 and Figures S6–S7).

3.4. Foreshock Kinematics

In the years preceding the ZES, the focal region is characterized by diffuse seismicity that highlights different local spatial clusters and different styles of faulting (Figures 3a and 3b and 5a). Most prominent clusters are found at about 37.5°N, 20.6°E, in the vicinity of the 2018 M_w 6.9 mainshock and close to the Peloponnese coastline, both onshore and offshore (Figures 3a–3b and 5a). The clusters appear to mostly delineate along a NW-SE direction (Figures 3a and 3b), marking known active faults both offshore western Peloponnese (Haddad et al., 2020; Kokkalas et al., 2013; Makris & Papoulia, 2014; Wardell et al., 2014) and onshore (Fountoulis et al., 2015), some of which have recently hosted large-magnitude historic earthquakes (e.g., the 1997 M_w 6.5 Strofades earthquake; Kiratzi & Louvari, 2003) (Figure 1). In addition to the NW-SE striking earthquake clusters, a NE-SW cluster in onshore Peloponnese appears to delineate the large NE-SW right-lateral strike-slip Movri Fault that produced the 2008 M6.4 Movri Earthquake (Figures 3a and 3b and Figures S2a and S2b) (Cesca et al., 2010; Konstantinou et al., 2009). This fault is active during the ZES
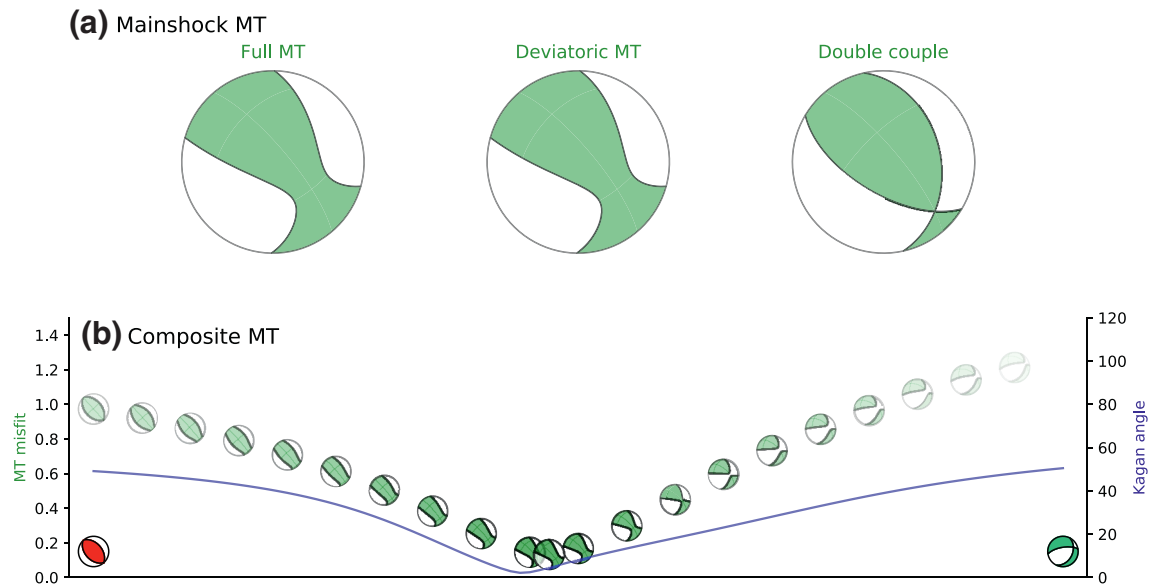
Figure 6. Mainshock moment tensor (MT) obtained. (a) Full MT obtained for the mainshock and its deviatoric and pure double couple (DC) components. (b) Overview of composite mainshock MT obtained superposing two MTs with different contributions, one for an earthquake (November 5, 2018 12:21) of the red thrust cluster and one for an earthquake (November 18, 2018 5:18) of the sea-green cluster; focal sphere are plotted with lower transparency as they better fit the mainshock full MT (a blue line, denoting the Kagan angle among double couples of the mainshock and composite MTs, shows that the DC is also well reproduced for the suggested MT composition).

foreshock sequence down to depths of ~20 km (Movie S1). Indeed, distinct deep (c. 0–20 km) and shallow (<5 km) seismicity clusters from June to November 2015 and from May to August 2016, respectively, highlight intermittent activity on sections of the Movri Fault (Movie S1 and Figure S20). The horizontal (dextral) sense of slip on this fault is further supported by the strike-slip focal mechanisms recorded along this structure prior to the main event (Figure 5a).

MT analysis (Figure 5) coupled with earthquake relocation (Figure 3) suggest that the early phase of the ZES involved slip on a series of steeply dipping NW-SE trending left-lateral strike-slip faults offshore western Peloponnese, at depths ranging from 15 to 20 km (see along-strike distance of 120–130 km on Profile A-A′ in Figure 3a). The predominantly sinistral strike-slip faulting is in agreement with focal mechanisms obtained by Haddad et al. (2020). In the following 3.5 years, seismicity migrated first eastward (toward onshore Peloponnese), involving strong interactions between faults immediately offshore and onshore western Peloponnese (Figures 3a and 3b) while earthquake activity west of Zakynthos was minimal, and from November 2015 until October 2018, the seismicity of the ZES migrated westward, toward the epicentral area of the M_w 6.9 event (Movie S1). During the entire foreshock sequence (January 01, 2014 to October 25, 2018), the ZES involved slip on mainly strike-slip and normal faults, with negligible contribution of thrust faulting (Figures 3a and 3b, Figure 5).

3.5. Mainshock and Aftershock Kinematics

The mainshock of the Zakynthos Earthquake is characterized by an oblique (thrust to strike-slip) mechanism. A full MT inversion suggests a significant nondouble-couple component (Figure 6), as proposed also by global catalogs (Global CMT) and previous studies (e.g., Sokos et al., 2020). This MT solution is compatible with the combination of two sources (as proposed also by Sokos et al., 2020), one characterized by thrust faulting, similar to those resolved for a cluster of aftershocks north of the mainshock hypocenter, and one by strike-slip to oblique mechanism, as found for several aftershocks east of the mainshock hypocenter (Figure 5b and Figure S3). These two individual sources share a common pressure axis with our overall MT solutions (Figure 5c and Figure 6). Our decomposition suggests a relatively steep dip angle (~45°) for the thrust subevent in agreement with Cirella et al. (2020), which could be compatible with a splay-thrust fault, and in contradiction to the low-dip angle suggested by Sokos et al. (2020) and Ganas et al. (2020), which

is more compatible with the plate-interface. Repeating our MT decomposition and forcing the thrust and strike-slip subevents to have the geometry proposed by Sokos et al. (2020), we find a significantly worse fit (Figure S8).

The aftershock sequence of the Zakynthos Earthquake appears outstanding in its heterogeneities. Seismicity spreads over about 60 km along the trench and 50 km across it (Figures 3c and 5b), and involves all types of earthquake mechanisms, including strike-slip, normal, thrust, and oblique faulting (Figure 5c), suggesting complex fault patterns on multiple faults of different depths and orientations. This is in agreement with local stress heterogeneities and fault diversity suggested for the study area by Konstantinou et al. (2017). The spatial distribution of the aftershocks presents two main trends: (i) the progressive localization of aftershocks toward the epicentral area of the main event (Figure 3c) and (ii) long-range (>50 km) interactions between the epicentral region and earthquakes occurring within clusters (i) and (ii) (Figure 3c). The latter fault interactions initiated ∼2 months after the mainshock and are animated in Movie S1.

The mainshock and some aftershocks (Figure 5b) suggest the rupture of an NNE-SSW striking and ESE-dipping (∼45°) thrust fault, which most likely reflects a thrust fault in the overriding plate (as opposed to the subduction plate-interface) (Figures 3, 5 and 6; Table S4), in agreement with results from Cirella et al. (2020). While our seismological results support the failure of a splay-thrust fault, we believe that seismological data alone cannot safely discriminate between the two scenarios because of the uncertainty on the depth and dip angle estimations for the aftershocks, as well as the ambiguity in the MT decomposition. However, the scenario of a splay-thrust fault is further supported here by published seismic reflection and bathymetric data (Figures 1 and 4, Figure S23) that reveal numerous ∼ NNW-SSE trending thrusts that dip 30°–50° to the northeast, beneath Zakynthos and western Peloponnese (Kokkalas et al., 2013; Makris & Papoulia, 2014; Sachpazi et al., 2000; Wardell et al., 2014; this study) and the recording of a minor (10 cm) tsunami along the western coastline of Peloponnese that suggests rupture of the sea-bed (Cirella et al., 2020). It is also supported by the low-dipping (<15°–17°) angle of the plate-interface beneath the epicentral area (e.g., Halpaap et al., 2018; Sachpazi et al., 2000). Nevertheless, the majority of the aftershocks mark the activation of other faults (Figure 5b). The location, depth, and focal mechanisms of the latter events are incompatible with both the mainshock rupture plane and the geometries recorded during the foreshock activity (Figures 3 and 5). Specifically, joint analysis of the location and mechanisms of the aftershock sequence suggests the activation of multiple steeply dipping strike-slip faults that run in ∼NE-SW orientations (and at high angles to the trench). The seismicity is confined above the subduction interface (<20 km) and deepens accordingly toward the coast of the Peloponnese (Figures 5e and 5f). A second family of events (red in Figures 5b–5f) denote reverse faulting along one or more additional NW-SE faults. It is noteworthy that focal mechanisms near the epicentral region (cluster iv in Figures 3a and 3b) mark a similar region as in the years preceding the main event, but with different mechanisms (Figure 5), suggesting that stress perturbations during the mainshock are able to inhibit strike-slip and oblique-normal mechanisms, which were dominant before October 25, 2018, and favor strike-slip and extensive thrust faulting. Fault slip reversed between the interseismic and postseismic periods has been also observed on crustal faults in Chile and is linked to the megathrust seismic cycle (Shirzaei et al., 2012).

4. Slow-Slip Events During the ZES

To assess the likely involvement of aseismic slip transients in the evolution of the ZES, we analyze the deformation on the Earth's surface recorded by 16 permanent Global Positioning System (GPS) stations located within the broader study area (Figure 1). We find that the earthquake activity within the ZES was accompanied by aseismic-slip release in the form of two slow-slip events (SSEs). Below, we first discuss the analysis and modeling of the GPS data and, following, we present evidence for two prominent GPS transient signals—which are the first SSEs to be recorded in the HSS.

4.1. GPS Time-Series Analysis and Modeling

Continuous GPS data with daily recordings were obtained from 16 permanent GPS stations located along western Peloponnese and the islands of Zakynthos and Kephalonia (Figures 1 and 7). We analyzed the ITRF08 daily coordinates of 11 stations (TRIP, RLSO, PYRG, PYL1, PAT0, KALM, KORI, MOL1, NEAB,

SPET, and VLSM) available at the Nevada Geodetic Laboratory, University of Nevada, Reno (NGL-UNR, http://geodesy.unr.edu/magnet.php; Blewitt et al., 2018) and of five stations (063A, 003A, 028A, 030A, 029A) that belong to the HEPOS network of the Hellenic Cadastre. Collectively, our GPS data set provides observations for a period of ~5.5 years (from January 01, 2014 till May 31, 2019) which is comparable to the time-period of the ZES (Figure 2e). The recordings at stations KALM, KORI, MOL1, PYRG, RLSO, SPET, and TRIP have, however, slightly shorter duration (see Figure 2e and Figures S9–S11). For more details on the geodetic data set used in this study, see Text S5 in the Supporting Information.

As a first step in our analysis, we removed outliers from the GPS signal by applying the Hampel filter, a common approach for reducing noise (Pearson, 2005) (Figures S9 and S10). Subsequently, we applied the Greedy Automatic Signal Decomposition algorithm (GrAtSiD; Bedford & Bevis, 2018) to decompose the GPS signal into (i) the seasonal oscillation signal, (ii) secular and transient motions, and (iii) the residual signal. The secular motion corresponds to the long-term velocity of the station, which is in principle stable, while the transient signal is estimated by fitting a minimum number of multitransient signals that are defined as the sum of two or more exponentially decaying time functions. Using the multitransient basis function, we can find a sparse number of other, unexpected signals, such as postseismic decays, subtle long-term interseismic accelerations (e.g., Heki & Mitsui, 2013; Loveless & Meade, 2016; Melnick et al., 2017), and short-term transients such as reversals (e.g., Bedford et al., 2020; Materna et al., 2019). The multitransient basis function approximates all of these unexpected signal types: its aim is to not perfectly fit each type of signal, although a good fit is desirable and it does tend to capture the main features reasonably well across all durations. The modeled trajectory signal (Figures S10–S12) is derived using a linear regression (see Bevis & Brown, 2014). The onset of the transient signal is not predefined, as GrAtSiD automatically detects possible transient onsets. We applied the GrAtSiD time-series decomposition using a station-by-station approach and, therefore, no assumptions are made on the spatial wavelength of transient signals. GrAtSiD was run on a component-by-component approach (Figures S10 and S11) to save on computational expense—this means that transients can begin at different times for different components at the same station. The convergence of the GrAtSiD algorithm was repeated 250 times in order to retrieve the optimum trajectory model (median; red lines in Figure S10) and uncertainty (interquartile range) of the 250 modeled trends resulting, thus, in a time-dependent estimate of the models' uncertainty. From the trajectory modeled signal, we isolate the transient signal (red lines in Figure S11) and subsequently we calculate the transient velocity signal for each station and over the entire network (Figure 2e). Transient daily velocities are recovered from the trajectory model by taking the differential of the trajectory model (minus the seasonal oscillations and steps). Two predominant changes in the network velocity are revealed in late 2014 and prior to the 2018 Zakynthos Earthquake (Figures 2e and Figure S13).

Transient signals in GPS time series may be tectonic (e.g., Wallace & Beavan, 2010) but may also be due to environmental or anthropogenic conditions, such as high precipitation rates or monument instability (Larson et al., 2008; Williams et al., 2004). To account for nontectonic signal, we assessed the maintenance history of all 16 stations used in this analysis as well as the fluid loading history in the area. The latter was predicted at each station location based on the ESMGFZ model (http://rz-vm115.gfz-potsdam.de:8080/repository), which produces values of elastic surface loading (Dill & Dobslaw, 2013). Transient signal in the fluid loading time series was modeled using GrAtSiD (Figure S15; for details see Text S5 in the Supporting Information). With respect to the long wavelength of fluid-loading signal, it appears that there is no strong correlation in space and/or time with the 2014–2015 and 2018 GPS transients (Figure S15). The only apparent correlation is found along the vertical component during the second GPS transient in 2018, which cannot rule out likely contribution of fluid loading to the instability of the system (e.g., Bedford et al., 2020). To further test for a likely nontectonic origin of the recorded transients, we searched for any systematic and/or periodical common-mode error related to the distortion of the reference frames. Analysis of three far-field stations (PVOG, SPAN, and LARM; data downloaded from the NGL-UNR), which are located outside the study area (see Figure 1, inset) clearly indicate that there are no transient signals during the time-period span by the ZES (Text S5 in the Supporting Information and Figure S16). Therefore, the recorded transients are very likely tectonic.

4.2. Slip Transients During the ZES

Tectonic transient signals in a GPS time series may be related to SSEs and/or postseismic relaxation (e.g., Sun et al., 2014). The latter possibility is excluded because there is no large ($M > 6$) earthquake in the fore-
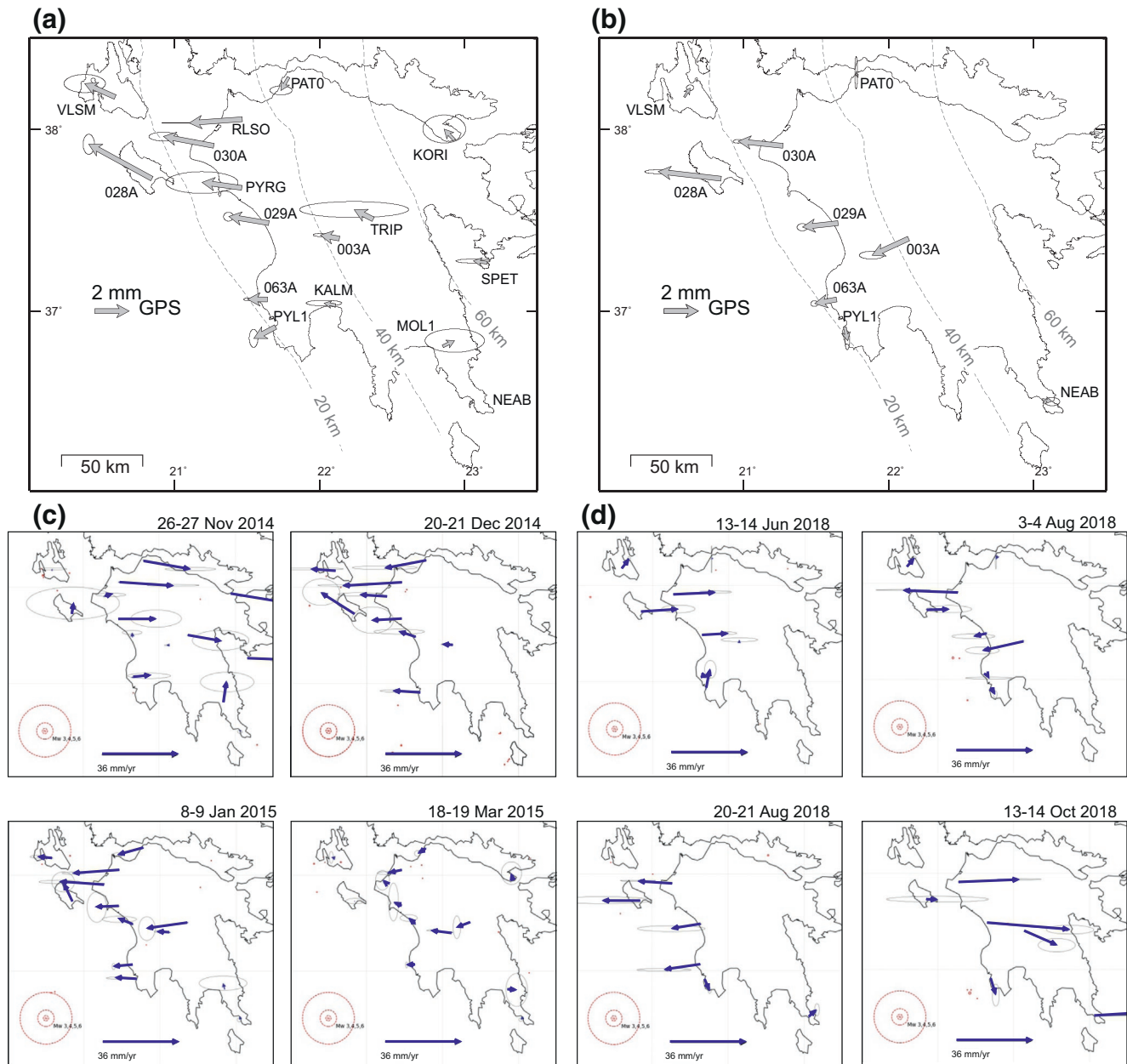
Figure 7. Slow-slip events (SSEs) along the termination of the Hellenic Subduction System. Transient signals of surface deformation as derived from the analysis of GPS time series. Cumulative trenchward transient displacements, together with their 1-sigma uncertainties, observed between (a) September 24, 2014 to March 20, 2015 and (b) May 14, 2018 to October 25, 2018. (c and d) Snapshots of the daily velocity evolution of the transient GPS signal with respect to the long-term velocity of each station for the periods corresponding to transient signals of (c and d), respectively. The upper-left panels in (c and d) show the network-wide acceleration observed before the reversal of the velocity vectors that follows (Figure 2e). Red circles represent earthquakes that scale with magnitude. Contours in (a and b) mark the top of the plate-interface (Halpaap et al., 2019).

shock sequence. To assess the spatiotemporal changes of the GPS velocity pattern within the study area, we calculate the daily median GPS network velocity along the east component, which is normal to the trench (Figure 2e). Examination of Figure 2e reveals two significant changes in the GPS velocities both associated with an eastward acceleration of the mean velocity of the vectors before their abrupt westward rotation (Figure 2e). The first of these transients occurs in late 2014 and lasts slightly more than 6 months, while the second starts in mid-2018 and continues until prior to the M_w 6.9 earthquake, lasting for about 5 months (Figures 2e and 7). Here, we need to clarify that although the transient signal lasts for about 6 and 5 months during the 2014 and 2018 episodes, respectively, the trench-ward motion that is associated with slow slip

has shorter duration (112 days in 2014 and 107 days in 2018; see Figure 2e and Text S5 in the Supporting Information). This is because each transient signal comprises individual deformational periods of different durations that include, successively, landward network acceleration, trenchward network acceleration (i.e., the SSE) and, for the 2018 transient, landward network acceleration until the main M_w 6.9 event (see below for details). Cumulative GPS displacements (Figures 7a and 7b) are estimated for the time-period over which vectors move trenchward while associated uncertainties are calculated using the law of error propagation (Mikhail, 1976). The daily evolution of these velocities, and the associated deformational periods within each transient, can be seen in Movie S2 whereas the interrelation between these SSEs and the seismic-moment release is highlighted in Movie S1.

The first transient initiates on September 24, 2014 and terminates at March 20, 2015 (that is, a total of 178 days) (Figure 2e and Movie S2). During this episode all near-field stations appear, first, to accelerate eastwards for about two months and, subsequently, to deviate from their main equilibrium position and rotate westwards (Figures 2e and 7a and 7c and Movie S2). The start of this transient is the start of the acceleration phase (as this is recorded in at least one station) whereas the end is the completion of the rotation of the vectors to their equilibrium position (see Movie S2). Maximum cumulative displacement of 4.2 ± 1.0 mm is recorded at station 028A in Zakynthos, while attenuated displacements are observed in eastern and southern Peloponnese (e.g., stations 030A, 063A, and TRIP; Figure 7). The small vector obliquity observed at station 028A in Zakynthos with respect to vectors in Peloponnese, possibly indicates the involvement in this slow-slip event of additional (mainly strike-slip) structures of offshore Peloponnese (e.g., Bürgmann, 2018). Microseismicity offshore/onshore western Peloponnese in late October 2014 temporarily coincides with the early stages of this SSE (Movie S2).

The second transient signal spans the time-period between May 14, 2018 and October 25, 2018 (~164 days), immediately preceding the M_w 6.9 Zakynthos Earthquake (Figure 2e). This SSE shows very similar characteristics to those recorded during the 2014–2015 transient (e.g., acceleration and trenchward rotation of the vectors; see Figures 2e and 7d and Movie S2). Here, the vector acceleration lasts also for ~2 months, followed by a trenchward rotation of the vectors (Figures 2e and 7 and Movie S2) and velocity acceleration until the Zakynthos mainshock (Figure 7d).

The start of the 2018 transient is the start of the acceleration phase (as this is recorded in at least one station) whereas the end is the Zakynthos mainshock (see Movie S2). Interestingly, here, station 028A at Zakynthos Island records each deformational phase (acceleration/rotation/readjustment and acceleration) with a time delay of ~30 days compared to the remaining stations (see Movie S2). This likely suggests an upward migration of slip from greater depths (beneath Peloponnese) to shallower depths (beneath Zakynthos). Similarly to the 2014 SSE, cumulative maximum displacement is observed on Zakynthos (station 028A) and is of comparable size (3.8 ± 1.0 mm) to the 2014 transient. This transient is associated with shallow (<10 km) seismic-moment release proximal to the epicentral area (Movie S1 and Figure S21).

The widespread occurrence of deformation along the entire western Peloponnese and Zakynthos Island, coupled with the trenchward orientation of the vectors (Figures 7a and 7b), collectively suggest that both transients likely originate on the subduction plate-interface that extends beneath central-western Peloponnese. To better explore the origin and spatial distribution of these two transients, we performed forward modeling and, assuming a homogeneous elastic half-space and using the analytical equations of Okada (1985), obtained surface displacements by assigning slip on the plate-interface (Figure S18). After testing for various displacement scenarios we derived, for each SSE, the best uniform-slip model by allowing average slip of 5 mm on the plate-interface (Figure S18c). The total geodetic moment released during each SSE is 3.20×10^{18} Nm and corresponds to a M_w ~6.3 earthquake (Table S1). The relationship between geodetic moment release/duration of the Zakynthos transients is similar to the relationships observed for other tectonic transient signals globally (Figure S19; Peng & Gomberg, 2010), reinforcing the tectonic origin of these deformational episodes. Some discrepancies observed in the north of the study area (Figure S18), likely reflect additional distributed slip on the plate-interface and/or upper-plate faults. Thus, the estimated average slip of 5 mm on the plate-interface should be considered as the minimum slip required for reproducing the observed surface deformation. Slip-inversion of the transient events will allow better assessment of their spatial distribution and is currently in progress (Saltogianni et al. Pers. Com). Furthermore, the acceleration of the vectors observed prior to both slow-slip events was recorded in all near-field stations to last for about

2 months in each case (Figures 2e and 7 and Movie S2). This acceleration may be indicative of deep active processes related to changes in slab pull force (Bedford et al., 2020) and/or to a dynamic increase of locking along the plate-interface zone prior to seismic or aseismic slip events (Materna et al., 2019). The described SSEs of this study are the first to be reported in the HSS.

5. The Preparatory Phase Leading to the M_w 6.9 Zakynthos Earthquake

Our data suggest that the *b*-values in the ZES systematically dropped below 1 soon after the trenchward rotation of the GPS velocity vectors during the 2014–2015 transient (Figures 2d and 2e and Figure S1c). Since that time, and until the main event in late 2018, the *b*-values in the ZES remained overall suppressed (<1), with one exception: the ~6 months (September 2016 to April 2017) where swarm-like microseismicity ruptured repeatedly the epicentral area accounting for high *b*-values (up to 1.36) and strong spatiotemporal earthquake clustering (Figure 3b, Figure S2c, and Movie S1); note that high *b*-values were again encountered only in the aftershock sequence (*b*~1.2; Figure 2d). Suppressed *b*-values (<1) have been observed prior to mainshocks globally (e.g., Nuannin et al., 2005; Schurr et al., 2014). On the other hand, elevated *b*-values (>1) often characterize aftershock sequences and/or earthquake swarms (Gulia et al., 2018; Scholz, 2015). The fluctuations recorded in the *b*-values of the ZES during the ~5 years preceding the mainshock are in accordance with these observations (Figure 2d), with low *b*-values (<1) most likely indicating increased stresses in the crust during the years preceding the main event (Schorlemmer et al., 2005).

Combining the above, we propose a scenario in which the SSE that occurred beneath western Peloponnese in late 2014, tectonically destabilized (*b* < 1) the western termination of the subduction system (while the forearc south of the study area continued to be characterized by *b*-values of ~1; Figure S1d) to, first, trigger swarm-like activity in the epicentral area of the mainshock in late 2016 and, subsequently, the M_w 6.9 Zakynthos Earthquake (Figures 2 and 3). As discussed in Section 4.2, it is likely that the first SSE involved, in addition to slip on the plate-interface, a triggered slow slip on one (or more) strike-slip structures in the upper-plate (see vector obliquity between Zakynthos/mainland in Figure 7a), a scenario that could promote widespread stress changes in the upper-plate (e.g., Hamling & Wallace, 2015). The persisting low (<1) *b*-values in the ZES after the first SSE and until the M_w 6.9 Zakynthos Earthquake about 4.5 years later, suggests significant stress perturbations which were not fully accommodated during the swarm seismic-moment release (equivalent to a ~M_w 4.9; Table S1) in the broader epicentral area of the Zakynthos mainshock. Interestingly, following these swarms, the epicentral area remained mostly quiet for the following year (from May 2017 to April 2018; Movie S1) before it becomes next active with the onset of the second transient in May 2018 (Movie S1 and Figure S20).

The second transient immediately precedes the main M_w 6.9 Zakynthos Earthquake (Figures 2d and 2e and 7b; Movie S2). The ~30 day phase-lag recorded in the reversal of the GPS vectors between Zakynthos (028A) and the rest of western Peloponnese (e.g., 030A, 029A, etc.), suggests the gradual up-dip migration of slip along the plate-interface, from ~40 km depth beneath Peloponnese to shallower crustal depths (<20 km) near Zakynthos (Figure 7d and Movie S2). It is possible for SSEs that operate either on the subduction plate-interface (Wallace & Beavan, 2010) or nearby crustal faults (Bürgmann, 2018; Hamling & Wallace, 2015), to trigger stress changes in the crust that would lead to generation of large-magnitude earthquakes. Whether this up-dip slip migration a few days before the mainshock produced static-stress changes on one or more upper-plate faults (King et al., 1994) capable of triggering the Zakynthos Earthquake, is investigated in a follow-up study (Saltogianni et al. Pers. Com).

6. Interplay Between Seismic and Aseismic Deformation at the Termination of the HSS

Our analysis records successive phases of seismic and aseismic deformation during the build-up to the M_w 6.9 Zakynthos Earthquake. One question that arises is what drives this type of deformation and how representative this may be in accommodating plate-motion over multiple earthquake-cycles. Slow-slip events that trigger swarm activity and/or moderate-to-large-sized earthquakes have been recorded before in major subduction zones globally, including New Zealand, Japan, Ecuador, Chile, and Mexico (Beavan et al., 2007; Colella et al., 2017; Kato et al., 2012; Obara & Kato, 2016; Ruiz et al., 2014; Vallée et al., 2013). Although

the detailed distribution of interseismic coupling beneath western Peloponnese in Greece has not been constrained, a first-order difference between the global examples and the Greek case is that the SSEs here occur on a weak plate-interface that largely creeps (Saltogianni et al., 2020; Vernant et al., 2014). The only other references for SSEs along creeping sections of the plate-interface (or sections with heterogeneous interseismic coupling) is at the central/northern Hikurangi margin in New Zealand (Wallace et al., 2016), in Ecuador (Vallee et al., 2013), Costa Rica (Davis et al., 2015), and the Boso Peninsula in Japan (Ozawa et al., 2007). In all these cases, however, the SSEs occur near the trench, at shallow (<10 km) sections of the plate-interface, and are accompanied by intense earthquake activity. By contrast, the SSEs at Zakynthos are deep (~20–40 km) and mostly seismicity free (Movie S1).

One possible explanation for the occurrence of aseismic transients at these depths of the HSS (i.e., 20–40 km) is that they mark the down-dip end of locally isolated locked patches (Lay, 2015). Such patches have been recently discovered south of Crete (Saltogianni et al., 2020) and between Crete and Peloponnese (Howell et al., 2017), where they locally appear to accumulate interseismic strain that may account for up to 85% of the plate-motion. Seismic tomography coupled with analysis of seismic attributes beneath the area of ZES suggests the existence of a high (~1.9) Vp/Vs ratio zone at crustal depths ranging between ~10 and 30 km (Halpaap et al., 2018), which is indicative of water-rich fluids (Audet et al., 2009) (Figure 8). As SSEs require very low effective stress (e.g., near lithostatic pore fluid pressures) and high fluid pressures (e.g., Gao & Wang, 2017; Liu & Rice, 2005), their presence beneath western Peloponnese is not surprising. Furthermore, studies have shown that fluids liberated from the plate-interface during SSEs tend to migrate upwards, into the lower portion of the seismogenic zone (Audet et al., 2009; Nakajima & Uchida, 2018) to trigger widespread microseismicity, often in the form of earthquake swarms. The network of strike-slip faults onshore/offshore western Peloponnese (Figures 1 and 4) is likely to have acted as conduits for fluid migration and triggering of microseismicity within the ZES (Figure 8), as it is the case with upper-plate faults elsewhere in the Hellenic forearc (Ruscic et al., 2019).

Recurring slow-slip events are common along subduction margins and in some cases (e.g., Nankai Trough megathrust) they appear to accommodate up to >50% of the total plate-motion (Araki et al., 2017). In Greece, two SSEs and significant microseismicity are recorded over a period of ~5 years to precede a large event (Figure 2d). A question that arises is what percentage of the plate-motion is accommodated by each process operating at the western-end of the HSS. To address this question, we have quantified the contribution of each component of deformation (seismic and aseismic) for the period that precedes the M_w 6.9 event (Table S5; for details refer to Text S6 in the Supporting Information). We find that the aseismic slip-rate (produced collectively by the two SSEs) amounts to ~2.1 mm/yr (or ~8% of the plate-motion), accommodating significantly more subduction-related strain compared to that produced by the ZES seismicity (slip-rate ~1.3 mm/yr or 5% of the plate-motion) (Table S5). These numbers collectively imply that during the ~5 years preceding the Zakynthos Earthquake, at least 15% of the plate-motion was released, ~70% was stored elastically (on upper-plate faults and/or the plate-interface), while the remaining ~15% was accommodated by aseismic creep along the downgoing plate (Table S5). The elevated (~70%) elastic strain reported here does not contradict the overall weak (<20%) locking reported for the Hellenic margin (Floyd et al., 2010; Reilinger et al., 2010; Saltogianni et al., 2020; Vernant et al., 2014). By contrast, knowing that the average locking along the Hellenic subduction interface is weak and that the crust beneath the ZES is broken up by numerous upper-plate faults (Figures 1, 4 and 8), we anticipate that a significant fraction of the 70% interseismic strain may be stored on one or more faults in the overriding plate (in addition to any strain stored within the plate-interface zone; Saltogianni et al., 2020). That was partly evident during the M_w 6.9 Zakynthos Earthquake which involved rupture of faults in the upper crust (Figure 8) and also during the aftershock sequence where seismic moment equivalent to ~ M_w 6.2 earthquake was accommodated by upper-plate faults (Table S1). Similar kinematics characterize the southern termination of the Hikurangi margin in New Zealand, where about 80% of the plate-motion (Wallace et al., 2012) and seismic-moment release during large-magnitude earthquakes (Mouslopoulou et al., 2019) are accommodated by upper-plate faults. Composite faulting patterns accompanied by alternating styles of deformation may characterize multifault subduction-termination zones. Our data support the view that the aseismic and seismic displacements observed within the ZES ~5 years prior to the M_w 6.9 Zakynthos Earthquake are probably manifestations of very late interseismic stress conditions (i.e., Schurr et al., 2014). Whether these features characterize the seismogenesis at the western termination
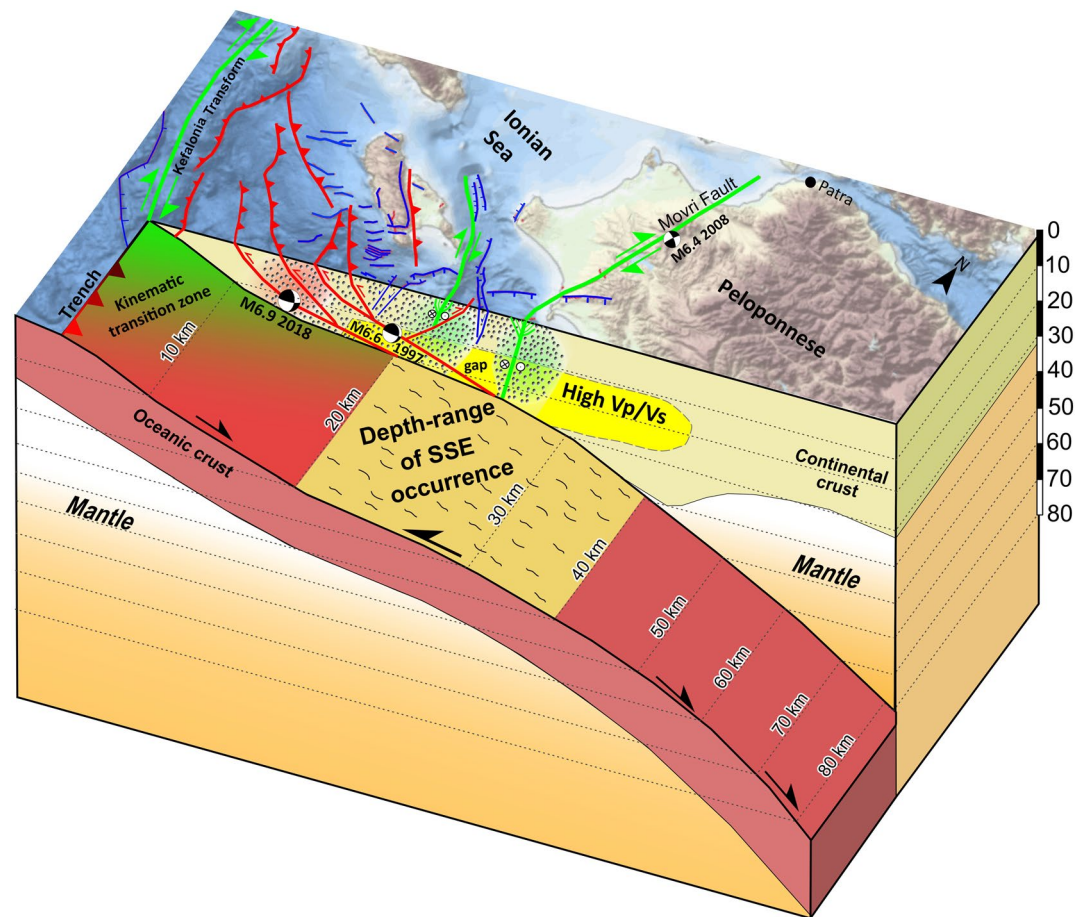
Figure 8. 3D-views of the deformation processes operating at the HSS termination. Schematic block diagram illustrating the spatial distribution of the seismic (earthquake) and aseismic (slow-slip events) deformation at the western-end of the Hellenic subduction margin as recorded during the 5 years preceding the M_w 6.9 Zakynthos Earthquake. Faults are color-coded according to fault type (red = thrust, blue = normal, green = strike-slip) as per Figures 1 and 3–5. The high Vp/Vs zone and the plate-interface contours derive from Halpaap et al. (2019). Shading around earthquakes highlights the larger clusters. The cross-section presented here partly reflects the seismic reflection line KY301-Z151A/B presented in Figure 4 (for location see Figure 1). The black moment tensor solutions indicate the two $M_w > 6$ earthquakes that ruptured two distinct thrust faults of the study area (see caption of Figure 1 for details). SSE, Slow slip event. Offshore bathymetry derived from EMODnet (https://portal.emodnet-bathymetry.eu/?menu=19).

of the HSS will be tested as additional data from future well-monitored large-magnitude earthquakes become available.

7. Conclusions

We have studied the deformation of the Earth's crust where active subduction zones terminate prior and after the 2018 M_w 6.9 Zakynthos Earthquake. Using earthquake, GPS, seismic reflection and bathymetric data, we find that the mainshock was preceded by a synergy of slow-slip events, earthquake swarms, and fault interactions between the subduction thrust and upper-plate faults that lasted about 5.5 years. This long-lasting preparatory phase initiated due to a plate-interface slow-slip event that released strain equivalent to a ~M_w 6.3 earthquake, tectonically destabilizing the upper 20–40 km of the crust and producing alternating phases of seismic and aseismic deformation between upper-plate faults and the plate-interface. Tectonic deformation included intense microseismicity ($M < 4$) on neighboring faults, earthquake swarms in the epicentral area of the mainshock, another episode of slow slip immediately preceding the mainshock and, eventually, the large (M_w 6.9) Zakynthos Earthquake. Tectonic instability in the area is evidenced by

a prolonged (∼3.5 years) period of overall supressed *b*-values (<1) and strong earthquake interactions on discrete strike-slip, thrust, and normal faults. Composite faulting patterns accompanied by alternating (seismic/aseismic) deformation styles may reflect late interseismic stress conditions prior to large-magnitude earthquakes that rupture subduction-termination zones.

Data Availability Statement

Available data from this work are archived in the online data repository https://doi.org/10.5281/zeno-do.4090118. The HEPOS geodetic data are restricted and are, therefore, not included in the above repository. In this analysis, we used seismological data from stations pertaining to the following networks: GE (GEOFON Data Centre, 1993), IU (ASL/USGS, 1988), II (SIO, 1986), G (IPGP & EOST, 1982), MN (Mednet, 1990), IV (INGV, 2006), HL (NOA, 1997), HT (AUTH, 1981), HP (UP, 2000), HA (UA, 2008), AC (IGEWE, 2002), 4A (Passarelli et al., 2012), X5 (Sokos, 2015); seismic data and metadata have been downloaded using the FDSN web services of Orfeus (https://www.orfeus-eu.org/data/eida/webservices/dataselect/), INGV (https://doi.org/10.13127/SD/X0FXNH7QFY), NOA (https://doi.org/10.7914/SN/HL), IRIS (https://service.iris.edu/fdsnws/), and Geofon (https://doi.org/10.14470/TR560404).

References

Albuquerque Seismological Laboratory (ASL)/USGS. (1988). *Global seismograph network*. IRIS/USGS International Federation of Digital Seismograph Networks (Dataset/Seismic Network). https://doi.org/10.7914/SN/IU

Anderson, H., & Jackson, J. (1987). Active tectonics of the Adriatic region. *Geophysical Journal of the Royal Astronomical Society*, *91*, 937–983.

Araki, E., Saffer, D., Kopf, A., Wallace, L., Kimura, T., Machida, Y., et al. (2017). Recurring and triggered slow-slip events near the trench at the Nankai Trough subduction megathrust. *Science*, *356*, 1157–1160. https://doi.org/10.1126/science.aan3120

Audet, P., Bostock, M. G., Christensen, N. I., & Peacock, S. M. (2009). Seismic evidence for overpressured subducted oceanic crust and megathrust fault sealing. *Nature*, *457*, 76–78. http://dx.doi.org/10.1038/nature07650

AUTH (Aristotle University of Thessaloniki). (1981). *Aristotle University of Thessaloniki seismological network*. International Federation of Digital Seismograph Networks. https://doi.org/10.7914/SN/HT

Beavan, J., Wallace, L., Douglas, A., & Fletcher, H. (2007). Slow slip events on the Hikurangi subduction interface, New Zealand. In P. Tregoning, & C. Rizos (Eds.), Dynamic planet: Monitoring and understanding a dynamic planet with geodetic and oceanographic tools (Vol. 130, pp. 438–444). Berlin, Germany: Springer.

Bedford, J., & Bevis, M. (2018). Greedy automatic signal decomposition and its application to daily GPS time series. *Journal of Geophysical Research: Solid Earth*, *123*, 6992–7003. https://doi.org/10.1029/2017JB014765

Bedford, J., Moreno, M., Deng, Z., Oncken, O., Schurr, B., John, T., et al. (2020). Months-long thousand-km-scale wobbling before great subduction earthquakes. *Nature*, *580*, 628–635.

Bevis, M., & Brown, A. (2014). Trajectory models and reference frames for crustal motion geodesy. *Journal of Geodesy*, *88*, 283–311.

Blewitt, G., Hammond, W. C., & Kreemer, C. (2018). Harnessing the GPS data explosion for interdisciplinary science. *Eos*, *99*. https://doi.org/10.1029/2018EO104623

Bouchon, M., Durand, V., Marsan, D., Karabulut, H., & Schmittbuhl, J. (2013). The long precursory phase of most large interplate earthquakes. *Nature Geoscience*, *6*, 299–302. https://doi.org/10.1038/ngeo1770

Bürgmann, R. (2018). The geophysics, geology, and mechanics of slow fault slip. *Earth and Planetary Science Letters*, *495*, 112–134.

Cesca, S. (2020). Seiscloud, a tool for density-based seismicity clustering and visualization. *Journal of Seismology*. https://doi.org/10.1007/s10950-020-09921-8

Cesca, S., Heimann, S., Stammler, K., & Dahm, T. (2010). Automated procedure for point and kinematic source inversion at regional distances. *Journal of Geophysical Research*, *115*. https://doi.org/10.1029/2009JB006450

Cesca, S., Rohr, A., & Dahm, T. (2013). Discrimination of induced seismicity by full moment tensor inversion and decomposition. *Journal of Seismology*, *17*(1), 147–163. https://doi.org/10.1007/s10950-012-9305-8

Cesca, S., Zhang, Y., Mouslopoulou, V., Wang, R., Saul, J., Savage, M., et al. (2017). Complex rupture process of the M_w 7.8, 2016, Kaikoura earthquake, New Zealand, and its aftershock sequence. *Earth and Planetary Science Letters*, *478*, 110–120.

Chousianitis, K., & Konca, A. O. (2019). Intraslab deformation and rupture of the entire subducting crust during the 25 October 2018 M_w 6.8 Zakynthos earthquake. *Geophysical Research Letters*, *46*. https://doi.org/10.1029/2019GL085845

Cirella, A., Romano, F., Avallone, A., Piatanesi, A., Briole, P., Ganas, A., et al. (2020). The 2018 M w 6.8 Zakynthos (Ionian Sea, Greece) earthquake: Seismic source and local tsunami characterization. *Geophysical Journal International*, *221*, 1043–1054.

Clément, C., Hirn, A., Charvis, P., Sachpazi, M., & Marnelis, F. (2000). Seismic structure and the active Hellenic subduction in the Ionian islands. *Tectonophysics*, *329*, 141–156.

Colella, H. V., Sit, S. M., Brudzinski, M. R., Graham, S. E., Demets, C., Holtkamp, S. G., et al. (2017). Seismicity rate increases associated with slow slip episodes prior to the 2012 M_w 7.4 Ometepec earthquake. *Earth and Planetary Science Letters*, *464*, 35–45.

Davis, E. E., Villinger, H., & Sun, T. (2015). Slow and delayed deformation and uplift of the outermost subduction prism following ETS and seismogenic slip events beneath Nicoya Peninsula, Costa Rica. *Earth and Planetary Science Letters*, *410*, 117–127.

Dill, R., & Dobslaw, H. (2013). Numerical simulations of global-scale high-resolution hydrological crustal deformations. *Journal of Geophysical Research: Solid Earth*, *118*, 5008–5017. https://doi.org/10.1002/jgrb.50353

Dziewonski, A. M., Chou, T.-A., & Woodhouse, J. H. (1981). Determination of earthquake source parameters from waveform data for studies of global and regional seismicity. *Journal of Geophysical Research*, *86*, 2825–2852. https://doi.org/10.1029/JB086iB04p02825

Ekström, G., Nettles, M., & Dziewonski, A. M. (2012). The global CMT project 2004-2010: Centroid-moment tensors for 13,017 earthquakes. *Physics of the Earth and Planetary Interiors*, *200–201*, 1–9. https://doi.org/10.1016/j.pepi.2012.04.002

Floyd, M. A., Billiris, H., Paradissis, D., Veis, G., Avallone, A., Briole, P., et al. (2010). A new velocity field for Greece: Implications for the kinematics and dynamics of the Aegean. *Journal of Geophysical Research*, *115*, B10403. https://doi.org/10.1029/2009JB007040

Fountoulis, I., Vassilakis, E., Mavroulis, S., Alexopoulos, J., Dilalos, S., & Erkeki, A. (2015). Synergy of tectonic geomorphology, applied geophysics and remote sensing techniques reveal the existence of active tectonism in NW Peloponnese (Greece). *Geomorphology*, *237*, 52–64.

Frohlich, C. (1992). Triangle diagrams: Ternary graphs to display similarity and diversity of earthquake focal mechanisms. *Physics of the Earth and Planetary Interiors*, *75*(1–3), 193–198. https://doi.org/10.1016/0031-9201(92)90130-N

Ganas, A., Briole, P., Bozionelos, G., Barberopoulou, A., Elias, P., Tsironi, V., et al. (2020). The 25 October 2018 M_w=6.7 Zakynthos earthquake (Ionian Sea, Greece): A low-angle fault model based on GNSS data, relocated seismicity, small tsunami and implications for the seismic hazard in the west Hellenic Arc. *Journal of Geodynamics*, *137*, 101731. https://doi.org/10.1016/j.jog.2020.101731

Gao, X., & Wang, K. (2017). Rheological separation of the megathrust seismogenic zone and episodic tremor and slip. *Nature*, *543*, 416–419.

GEOFON Data Centre. (1993). *GEOFON seismic network*. Deutsches GeoForschungsZentrum GFZ. https://doi.org/10.14470/TR560404

Gulia, L., Rinaldi, A. P., Tormann, T., Vannucci, G., Enescu, B., & Wiemer, S. (2018). The effect of a mainshock on the size distribution of the aftershocks. *Geophysical Research Letters*, *45*, 13277–13287. https://doi.org/10.1029/2018GL080619

Haddad, A., Ganas, A., Kassaras, I., & Lupi, M. (2020). Seismicity and geodynamics of western Peloponnese and central Ionian Islands: Insights from a local seismic deployment. *Tectonophysics*, *778*, 228353. https://doi.org/10.1016/j.tecto.2020.228353

Halpaap, F., Rondenay, S., & Ottemöller, L. (2018). Seismicity, deformation, and metamorphism in the Western Hellenic Subduction Zone: New constraints from tomography. *Journal of Geophysical Research: Solid Earth*, *123*, 3000–3026. https://doi.org/10.1002/2017JB015154

Halpaap, F., Rondenay, S., Perrin, A., Goes, S., Ottemöller, L., Austrheim, H. O., et al. (2019). Earthquakes track subduction fluids from slab source to mantle wedge sink. *Science Advances*, *5*. https://doi.org/10.1126/sciadv.aav7369

Hamling, I. J., & Wallace, L. M. (2015). Silent triggering: Aseismic crustal faulting induced by a subduction slow slip event. *Earth and Planetary Science Letters*, *421*, 13–19. https://doi.org/10.1016/j.epsl.2015.03.046

Heimann, S., Isken, M., Kühn, D., Sudhaus, H., Steinberg, A., Vasyura-Bathke, H., et al. (2018). *Grond—A probabilistic earthquake source inversion framework*. V. 1.0. GFZ Data Services. https://doi.org/10.5880/GFZ.2.1.2018.003

Heki, K., & Mitsui, Y. (2013). Accelerated Pacific Plate subduction following interplate thrust earthquakes at the Japan Trench. *Earth and Planetary Science Letters*, *363*, 44–49.

Howell, A., Palamartchouk, K., Papanikolaou, X., Paradissis, D., Raptakis, C., Copley, A., et al. (2017). The 2008 Methoni earthquake sequence: The relationship between the earthquake cycle on the subduction interface and coastal uplift in SW Greece. *Geophysical Journal International*, *208*(3), 1592–1610. https://doi.org/10.1093/gji/ggw462

IGEWE (Institute of Geosciences, Energy, Water and Environment). (2002). *Albanian seismological network*. International Federation of Digital Seismograph Networks (Dataset/Seismic Network). https://doi.org/10.7914/SN/AC

INGV Seismological Data Centre. (2006). *Rete Sismica Nazionale (RSN)*. Italy: Istituto Nazionale di Geofisica e Vulcanologia (INGV). https://doi.org/10.13127/SD/X0FXNH7QFY

Institut De Physique Du Globe De Paris (IPGP), & Ecole Et Observatoire Des Sciences De La Terre De Strasbourg (EOST). (1982). *GEOSCOPE, French Global Network of broad band seismic stations*. Institut de Physique du Globe de Paris (IPGP). https://doi.org/10.18715/GEOSCOPE.G

Karastathis, V. K., Mouzakiotis, E., Ganas, A., & Papadopoulos, G. A. (2015). High-precision relocation of seismic sequences above a dipping Moho: The case of the January-February 2014 seismic sequence on Cephalonia island (Greece). *Solid Earth*, *6*, 173–184.

Kassaras, I., Kapetanidis, V., & Karakonstantis, A. (2016). On the spatial distribution of seismicity and the 3D tectonic stress field in western Greece. *Physics and Chemistry of the Earth*, *95*, 50–72.

Kato, A., Obara, K., Igarashi, T., Tsuruoka, H., Nakagawa, S., & Hirata, N. (2012). Propagation of slow slip leading up to the 2011 M_w 9.0 Tohoku-Oki earthquake. *Science*, *335*, 705–708.

King, G. C., Stein, R. S., & Lin, J. (1994). Static stress changes and the triggering of earthquakes. *Bulletin of the Seismological Society of America*, *84*, 935–953.

Kiratzi, A., & Louvari, E. (2003). Focal mechanisms of shallow earthquakes in the Aegean Sea and the surrounding lands determined by waveform modelling: A new database. *Journal of Geodynamics*, *36*, 251–274.

Kokinou, E., Kamberis, E., Vafidis, A., Monopolis, D., Ananiadis, G., & Zelilidis, A. (2005). Deep seismic reflection data from offshore western Greece: A new crustal model for the Ionian Sea. *Journal of Petroleum Geology*, *28*, 185–202.

Kokkalas, S., Kamberis, E., Xypolias, P., Sotiropoulos, S., & Koukouvelas, I. (2013). Coexistence of thin-and thick-skinned tectonics in Zakynthos area (Western Greece): Insights from seismic sections and regional seismicity. *Tectonophysics*, *597–598*, 73–84. https://doi.org/10.1016/j.tecto.2012.08.004

Konstantinou, K. I., Melis, N. S., Lee, S. J., Evangelidis, C. P., & Boukouras, K. (2009). Rupture process and aftershocks relocation of the 8 June 2008 M_w 6.4 earthquake in northwest Peloponnese, western Greece. *Bulletin of the Seismological Society of America*, *99*, 3374–3389. https://doi.org/10.1785/0120080301

Konstantinou, K. I., Mouslopoulou, V., Liang, W.-T., Heidbach, O., Oncken, O., & Suppe, J. (2017). Present-day crustal stress field in Greece inferred from regional-scale damped inversion of earthquake focal mechanisms. *Journal of Geophysical Research: Solid Earth*, *122*, 506–523. https://doi.org/10.1002/2016JB013272

Larson, K. M., Small, E. E., Gutmann, E. D., Bilich, A. L., Braun, J. J., & Zavorotny, V. U. (2008). Use of GPS receivers as a soil moisture network for water cycle studies. *Geophysical Research Letters*, *35*, L24405. https://doi.org/10.1029/2008GL036013

Lay, T. (2015). The surge of great earthquakes from 2004 to 2014. *Earth and Planetary Science Letters*, *409*, 133–146.

Liu, Y., & Rice, J. R. (2005). Aseismic slip transients emerge spontaneously in three dimensional rate and state modeling of subduction earthquake sequences. *Journal of Geophysical Research*, *110*, B08307. https://doi.org/10.1029/2004JB003424

Lomax, A., Virieux, J., Volant, P., & Berge-Thierry, C. (2000). Probabilistic earthquake location in 3D and layered models. In C. H. Thurber, & N. Rabinowitz (Eds.), *Advances in seismic event location* (pp. 101–134). Dordrecht, Amsterdam, The Netherlands: Springer, Kluwer.

Louvari, E., Kiratzi, A., & Papazachos, B. (1999). The Cephalonia Transform Fault and its continuation to western Lefkada Island. *Tectonophysics*, *308*, 223–236. https://doi.org/10.1016/S0040-1951(99)00078-5

Loveless, J. P., & Meade, B. J. (2016). Two decades of spatiotemporal variations in subduction zone coupling offshore Japan. *Earth and Planetary Science Letters*, *436*, 19–30.

Makris, J., & Papoulia, J. (2014). The backstop between the Mediterranean Ridge and western Peloponnese, Greece: Its crust and tectonization. An active seismic experiment with ocean bottom seismographs. *Bollettino di Geofisica Teorica e Applicata*, *55*, 249–279. https://doi.org/10.4430/bgta0125

Mann, P., & Frohlich, C. (1999). *Classification and tectonic comparison of subduction to strike-slip transitions on active plate boundaries*. Paper presented at Penrose Conference on Subduction to Strike-Slip Transitions on Plate Boundaries, Geological Society of America, Puerto Plata, Dominican Republic.

Materna, K., Bartlow, N., Wech, A., Williams, C., & Bürgmann, R. (2019). Dynamically triggered changes of plate interface coupling in Southern Cascadia. *Geophysical Research Letters*, *46*, 12890–12899. https://doi.org/10.1029/2019GL084395

McClusky, S., Balassanian, S., Barka, A., Demir, C., Ergintav, S., Georgiev, I., et al. (2000). Global Positioning System constraints on plate kinematics and dynamics in the eastern Mediterranean and Caucasus. *Journal of Geophysical Research*, *105*(B3), 5695–5719. https://doi.org/10.1029/1999JB900351

MedNet Project Partner Institutions. (1990). *Mediterranean very broadband seismographic network (MedNet)*. Istituto Nazionale di Geofisica e Vulcanologia (INGV). https://doi.org/10.13127/SD/FBBBTDTD6Q

Melnick, D., Moreno, M., Quinteros, J., Baez, J. C., DengLi, Z. S., & Oncken, O. (2017). The super-interseismic phase of the megathrust earthquake cycle in Chile. *Geophysical Research Letters*, *44*, 784–791. https://doi.org/10.1002/2016GL071845

Mikhail, E. M. (1976). *Observations and least squares*. New York, NY: IEP—A Dun-Donnelley Publisher.

Mouslopoulou, V., & Hristopulos, D. T. (2011). Patterns of tectonic fault interactions captured through variogram analyses of microearthquakes. *Journal of Geophysical Research*, *116*, B07305. https://doi.org/10.1029/2010JB007804

Mouslopoulou, V., Nicol, A., Begg, J., Oncken, O., & Moreno, M. (2015). Clusters of mega-earthquakes on upper plate faults control the Eastern Mediterranean hazard. *Geophysical Research Letters*, *42*, 10282–10289. https://doi.org/10.1002/2015GL066371

Mouslopoulou, V., Saltogianni, V., Nicol, A., Oncken, O., Begg, J., Babeyko, A., et al. (2019). Breaking a subduction-termination from top-to-bottom: The 2016 Kaikōura earthquake, New Zealand. *Earth and Planetary Science Letters*, *506*, 221–230. https://doi.org/10.1016/j.epsl.2018.10.020

Nakajima, J., & Uchida, N. (2018). Repeated drainage from megathrusts during episodic slow slip. *Nature Geoscience*, *11*, 351–356.

NOA (National Observatory of Athens), Institute of Geodynamics, Athens. (1997). *National observatory of Athens seismic network*. International Federation of Digital Seismograph Networks (Dataset/Seismic Network). https://doi.org/10.7914/SN/HL

Nuannin, P., Kulhánek, O., & Persson, L. (2005). Spatial and temporal b-value anomalies preceding the devastating off coast of NW Sumatra earthquake of December 26, 2004. *Geophysical Research Letters*, *32*, L11307. https://doi.org/10.1029/2005GL022679

Obara, K., & Kato, A. (2016). Connecting slow earthquakes to huge earthquakes. *Science*, *353*, 253–257.

Okada, Y. (1985). Surface deformation due shear and tensile faults in a half-space. *Bulletin of the Seismological Society of America*, *75*, 1135–1154.

Ozawa, S., Suito, H., Imakiire, T., & Murakami, M. (2007). Spatiotemporal evolution of aseismic interplate slip between 1996 and 1998 and between 2002 and 2004, in Bungo channel, southwest Japan. *Journal of Geophysical Research*, *112*, B05409. https://doi.org/10.1029/2006JB004643

Papazachos, B., & Papazachou, C. (2003). *The earthquakes of Greece*: Ziti Publication.

Passarelli, L., Roessler, D., Aladino, G., Maccaferri, F., Moretti, M., Lucente, F. P., et al. (2012). *Pollino seismic experiment (2012-2014)*. Deutsches GeoForschungsZentrum GFZ. https://doi.org/10.14470/9N904956

Pearce, D., Rondenay, S., Sachpazi, M., Charalampakis, M., & Royden, L. H. (2012). Seismic investigation of the transition from continental to oceanic subduction along the western Hellenic subduction Zone. *Journal of Geophysical Research*, *117*, 1–18. https://doi.org/10.1029/2011JB009023

Pearson, K. R. (2005). *Mining imperfect data: Dealing with contamination and incomplete records* (p. 312): SIAM.

Peng, Z., & Gomberg, J. (2010). An integrated perspective of the continuum between earthquakes and slow-slip phenomena. *Nature Geoscience*, *3*, 599–607. https://doi.org/10.1038/ngeo940

Pérouse, E., Sébrier, M., Braucher, R., Chamot-Rooke, N., Bourlès, D., Briole, P., et al. (2017). Transition from collision to subduction in Western Greece: The Katouna–stamna active fault system and regional kinematics. *International Journal of Earth Sciences*, *106*, 967–989. https://doi.org/10.1007/s00531-016-1345-9

Reilinger, R., McClusky, S., Paradissis, D., Ergintav, S., & Vernant, P. (2010). Geodetic constraints on the tectonic evolution of the Aegean region and strain accumulation along the Hellenic subduction zone. *Tectonophysics*, *488*(1–4), 22–30. https://doi.org/10.1016/j.tecto.2009.05.027

Royden, L. H. & Papanikolaou, D. J. (2011). Slab segmentation and late Cenozoic disruption of the Hellenic arc. *Geochemistry, Geophysics, Geosystems*, *12*. https://doi.org/10.1029/2010GC003280

Ruiz, S., Metois, M., Fuenzalida, A., Ruiz, J., Leyton, F., Grandin, R., et al. (2014). Intense foreshocks and a slow slip event preceded the 2014 Iquique M_w 8.1 earthquake. *Science*, *345*, 165–1169. http://dx.doi.org/10.1126/science1256074

Ruscic, M., Bocchini, G. M., Becker, D., Meier, T., & van Keken, P. E. (2019). Variable spatio-temporal clustering of microseismicity in the Hellenic Subduction Zone as possible indicator for fluid migration. *Lithos*, *346*, 105154.

Sachpazi, M., Hirn, A., Clément, C., Haslinger, F., Laigle, M., Kissling, E., et al. (2000). Western Hellenic subduction and Cephalonia Transform: Local earthquakes and plate transport and strain. *Tectonophysics*, *319*, 301–319.

Saltogianni, V., Mouslopoulou, V., Oncken, O., Nicol, A., Gianniou, M., & Mertikas, S. (2020). Elastic fault interactions and earthquake-rupture along the southern Hellenic subduction plate-interface zone in Greece. *Geophysical Research Letters*, *47*, e2019GL086604. https://doi.org/10.1029/2019GL086604

Scholz, C. H. (2015). On the stress dependence of the earthquake *b* value. *Geophysical Research Letters*, *42*, 1399–1402. https://doi.org/10.1002/2014GL062863

Schorlemmer, D., Wiemer, S., & Wyss, M. (2005). Variations in earthquake-size distribution across different stress regimes. *Nature*, *437*(539), 542. https://doi.org/10.1038/nature04094

Schurr, B., Asch, G., Hainzl, S., Bedford, J., Hoechner, A., Palo, M., et al. (2014). Gradual unlocking of plate boundary controlled initiation of the 2014 Iquique earthquake. *Nature*, *512*, 299–302.

Shirzaei, M., Burgmann, R., Oncken, O., Walter, T. R., Victor, P., & Ewiak, O. (2012). Response of forearc crustal faults to the megathrust earthquake cycle: InSAR evidence from mejillones Peninsula, Northern Chile. *Earth and Planetary Science Letters*, *333–334*, 157–164.

SIO (Scripps Institution of Oceanography). (1986). *Global seismograph network*. IRIS/IDA International Federation of Digital Seismograph Networks (Dataset/Seismic Network). https://doi.org/10.7914/SN/II

Sokos, E. (2015). *Lefkada temporary network*. International Federation of Digital Seismograph Networks (Dataset/Seismic Network). https://doi.org/10.7914/SN/X5_2015

Sokos, E., Gallovič, F., Evangelidis, C. P., Serpetsidaki, A., Plicka, V., Kostelecký, J., et al. (2020). The 2018 M$_w$ 6.8 Zakynthos, Greece, earthquake: Dominant strike-slip faulting near subducting slab. *Seismological Research Letters*, *91*, 721–732. https://doi.org/10.1785/0220190169

Storchak, D. A., Di Giacomo, D., Bondár, I., Engdahl, E. R., Harris, J., Lee, W. H., et al. (2013). Public release of the ISC–GEM global instrumental earthquake catalogue (1900–2009). *Seismological Research Letters*, *84*, 810–815.

Sun, T., Wang, K., Iinuma, T., Hino, R., He, J., & Fujimoto, H., et al. (2014). Prevalence of viscoelastic relaxation after the 2011 Tohoku-oki earthquake. *Nature*, *514*, 84–87.

UA (University of Athens). (2008). *Hellenic seismological network, University of Athens, Seismological Laboratory*. International Federation of Digital Seismograph Networks (Dataset/Seismic Network). https://doi.org/10.7914/SN/HA

Uchida, N., Iinuma, T., NadeauBürgmann, R. M. R., & Hino, R. (2016). Periodic slow slip triggers megathrust zone earthquakes in northeastern Japan. *Science*, *351*, 488–492.

UP (University of Patras). (2000). *University of Patras, Seismological Laboratory*. International Federation of Digital Seismograph Networks (Dataset/Seismic Network). https://doi.org/10.7914/SN/HP

Vallee, M., Nocquet, J. M., Battaglia, J., Font, Y., Segovia, M., Régnier, M., et al. (2013). Intense interface seismicity triggered by a shallow slow slip event in the Central Ecuador subduction zone. *Journal of Geophysical Research: Solid Earth*, *118*, 2965–2981. https://doi.org/10.1002/jgrb.50216

Vernant, P., Reilinger, R., & McClusky, S. (2014). Geodetic evidence for low coupling on the Hellenic subduction plate interface. *Earth and Planetary Science Letters*, *385*, 122–129. https://doi.org/10.1016/j.epsl.2013.10.018

Waldhauser, F., & Ellsworth, W. L. (2002). Fault structure and mechanics of the Hayward Fault, California, from double-difference earthquake locations. *Journal of Geophysical Research*, *107*. https://doi.org/10.1029/2000JB000084

Wallace, L. M., Barnes, P., Beavan, J., Van Dissen, R., Litchfield, N., Mountjoy, J., et al. (2012). The kinematics of a transition from subduction to strike-slip: An example from the central New Zealand plate-boundary. *Journal of Geophysical Research*, *117*, B02405. https://doi.org/10.1029/2011JB008640

Wallace, L. M., & Beavan, J. (2010). Diverse slow slip behavior at the Hikurangi subduction margin, New Zealand. *Journal of Geophysical Research*, *115*, B12402. http://dx.doi.org/10.1029/2010JB007717

Wallace, L. M., Webb, S. C., Ito, Y., Mochizuki, K., Hino, R., & Henrys, S., et al. (2016). Slow slip near the trench at the Hikurangi subduction zone. *Science*, *352*, 701–704.

Wardell, N., Camera, L., Mascle, J., Nicolich, R., Marchi, M., & Barison, E. (2014). The structural framework of the Peloponnese continental margin from Zakynthos to Pylos from seismic reflection and morpho-bathymetric data. *Bollettino di Geofisica Teorica e Applicata*, *55*, 343–367. https://doi.org/10.4430/bgta0087

Williams, S. D. P., Bock, Y., Fang, P., Jamason, P., Nikolaidis, R. M., Prawirodirdjo, L., et al. (2004). Error analysis of continuous GPS position time series. *Journal of Geophysical Research*, *109*, 1–19. https://doi.org/10.1029/2003JB002741

References From the Supporting Information

1. Aki, K. (1966). *Generation and propagation of G waves from the Niigata earthquake of June 16, 1964: Part 2. Estimation of earthquake moment, released energy, and stress-strain drop from the G wave spectrum* (Vol. 44, pp. 73–88): Bulletin of the Earthquake Research Institute, University of Tokyo.

2. Bassin, C., Laske, G., & Masters, G. (2000). The current limits of resolution for surface wave tomography in North America. *Eos Transactions American Geophysical Union*, *81*, F897.

3. Calais, E. (1999). Continuous GPS measurements across the western Alps, 1996–1998. *Geophysical Journal International*, *138*, 221–230.

4. Dong, D., Fang, P., Bock, Y., Webb, F., Prawirodirdjo, L., Kedar, S., & Jamason, P. (2006). Spatiotemporal filtering using principal componentanalysis and Karhunen-Loeve expansion approaches for regional GPS network analysis. *Journal of Geophysical Research*, *111*, B03405. https://doi.org/10.1029/2005JB003806

5. Grigoli, F., Cesca, S., Rinaldi, A. P., Manconi, A., Lopez Comino, J. A., Clinton, J.F., et al. (2018). The November 2017 M$_w$ 5.5 Pohang earthquake: A possible case of induced seismicity in South Korea. *Science*, *360*(6392), 1003–1006. https://doi.org/10.1126/science.aat2010

6. Hanks, T. C., & Kanamori, H. (1979). A moment magnitude scale. *Journal of Geophysical Research*, *84*, 2348–2350.

7. Kennett, B. L. N., Engdahl, E. R., & Buland, R. (1995). Constraints on seismic velocities in the earth from travel times. *Geophysical Journal International*, *122*, 108–124.

8. Lomax, A., Michelini, A., & Curtis, A. (2009). Earthquake location, direct, global-search methods. In R. A. Meyers (Ed.), *Encyclopedia of complexity and systems science* (pp. 2449–2473). New York, NY: Springer.

9. Moschas, F., Avallone, A., Saltogianni, V., & Stiros, S. C. (2014). Strong motion displacement waveforms using 10-Hz precise point positioning GPS: An assessment based on free oscillation experiments. *Earthquake Engineering Structure Dynamics*, *43*, 1853–1866. https://doi.org/10.1002/eqe.2426

10. Negi, S. S., Paul, A., Cesca, S., Kamal, Kriegerowski, M., Mahesh, P., & Gupta, S. (2017). Crustal velocity structure and earthquake processes of Garhwal-Kumaun Himalaya: Constraints from regional waveform inversion and array beam modeling. *Tectonophysics*, *712*, 45–63. https://doi.org/10.1016/j.tecto.2017.05.007

11. Serpelloni, E., Faccenna, C., Spada, G., Dong, D., & Williams, S. D. P. (2013). Vertical GPS ground motion rates in the Euro-Mediterranean region: New evidence of velocity gradients at different spatial scales along the Nubia-Eurasia plate boundary. *Journal of Geophysical Research: Solid Earth*, *118*, 6003–6024. https://doi.org/10.1002/2013JB010102

12. Tetreault, P., Kouba, J., Heroux, P., & Legree, P. (2005). CSRS-PPP: An internet service for GPS user access to the Canadian Spatial Reference frame. *Geomatica*, *59*, 17–28.

13. Utsu, T. (1965). A method for determining the value of b in a formula 329 log $n=a-bM$ showing the magnitude-frequency relation for 330 earthquakes. *Geophysical Bulletin of Hokkaido University*, *13*, 99–103.

14. Wiemer, S., & Wyss, M. (2000). Minimum magnitude of completeness in earthquake catalogs: Examples from Alaska, the Western United States, and Japan. *Bulletin of the Seismological Society of America*, *90*, 859–869.